

# Electrical Resistivity Tomography Monitoring of In Situ Soil Flushing at the Hanford 100-K East Area

100KE Soil Flushing Monitoring

March 2024

Tim Johnson  
Jon Thomle  
Judy Robinson  
Rob Mackley

## DISCLAIMER

This report was prepared as an account of work sponsored by an agency of the United States Government. Neither the United States Government nor any agency thereof, nor Battelle Memorial Institute, nor any of their employees, makes **any warranty, express or implied, or assumes any legal liability or responsibility for the accuracy, completeness, or usefulness of any information, apparatus, product, or process disclosed, or represents that its use would not infringe privately owned rights.** Reference herein to any specific commercial product, process, or service by trade name, trademark, manufacturer, or otherwise does not necessarily constitute or imply its endorsement, recommendation, or favoring by the United States Government or any agency thereof, or Battelle Memorial Institute. The views and opinions of authors expressed herein do not necessarily state or reflect those of the United States Government or any agency thereof.

PACIFIC NORTHWEST NATIONAL LABORATORY  
*operated by*  
BATTELLE  
*for the*  
UNITED STATES DEPARTMENT OF ENERGY  
*under Contract DE-AC05-76RL01830*

Printed in the United States of America

Available to DOE and DOE contractors from  
the Office of Scientific and Technical Information,  
P.O. Box 62, Oak Ridge, TN 37831-0062

[www.osti.gov](http://www.osti.gov)

ph: (865) 576-8401

fox: (865) 576-5728

email: [reports@osti.gov](mailto:reports@osti.gov)

Available to the public from the National Technical Information Service  
5301 Shawnee Rd., Alexandria, VA 22312

ph: (800) 553-NTIS (6847)

or (703) 605-6000

email: [info@ntis.gov](mailto:info@ntis.gov)

Online ordering: <http://www.ntis.gov>

# **Electrical Resistivity Tomography Monitoring of In Situ Soil Flushing at the Hanford 100-K East Area**

100KE Soil Flushing Monitoring

March 2024

Tim Johnson  
Jon Thomle  
Judy Robinson  
Rob Mackley

Prepared for  
the U.S. Department of Energy  
under Contract DE-AC05-76RL01830

Pacific Northwest National Laboratory  
Richland, Washington 99354

## Summary

*In situ* soil flushing was tested at the Hanford 100-KE Area to accelerate the removal of the residual hexavalent chromium [Cr(VI)] contamination in the vadose zone. Soil flushing works by applying clean flush water at the surface, which mobilizes and transports Cr(VI) as it migrates downward to top of the groundwater aquifer (water table). Once the Cr(VI) reaches the groundwater, it is hydraulically contained, extracted, and treated through groundwater pump and treat operations. The efficacy of soil flushing is directly related to the volume and distribution of water that infiltrates through contaminated soils and mobilizes Cr(VI). Therefore, performance monitoring requires an understanding of flush water migration through the vadose zone.

It is challenging to comprehensively assess soil flushing performance via traditional vadose zone boreholes due to the limited volume of investigation afforded by a given borehole. As an alternative, 3D time-lapse electrical resistivity tomography (ERT) was tested as a method of monitoring the distribution of flush water over time within the vadose zone below the treatment area. ERT is a method of imaging the bulk electrical conductivity of the subsurface, which is highly dependent on water saturation levels in unconsolidated and unsaturated sediments. Thus, the timing and location of changes in bulk conductivity caused by soil flushing can be used to infer flush water migration pathways.

This report presents results of 3D time-lapse ERT imaging during two separate soil flushing campaigns conducted during the spring and summer months of 2022 and 2023. Results show generally that:

1. Pit backfill materials appear to have larger permeability than native (undisturbed) soils. Consequently, the boundary between pit backfill and native soil had a significant impact on flush water migration, causing some flush water to migrate along the pit boundary toward the bottom of the pit.
2. Non-uniform flows, likely caused by variations in physical or hydraulic properties in the pit backfill materials, resulted in uneven flush water distribution on the southern margin of the soil flushing zone.
3. Redistribution of water at the interface between backfill materials and the underlying Hanford formation sediments likely facilitated enhanced flushing within native soils beneath the deeper parts of the pit boundary, which presumably overlies soils with elevated Cr(VI) contamination. These areas appear to have been infiltrated by higher volumes of flush water than the northern and southern margins of the flush zone.
4. In comparison to 2022, high flush water application rates used in 2023 significantly improved flush water distribution throughout the target flushing zone.
5. Imaging resolution was limited to a depth of ~20 meters below the ground surface, due primarily to limitations on the lateral extent of the surface ERT array (depth of investigation is proportional to the lateral footprint of the ERT array). The ~10-meter region of the vadose zone between ~130 meters elevation and the water table at ~120 meters elevation was unresolved.

Figure S.1 shows an example ERT image along three cross-sections that represent the maximum flush water distribution for the 2022 and 2023 soil flushing campaigns. Each image demonstrates the variability in flush water distribution caused by subsurface heterogeneity, particularly in 2022, and the improvement in flush water distribution at the higher flush water application rate applied in 2023.

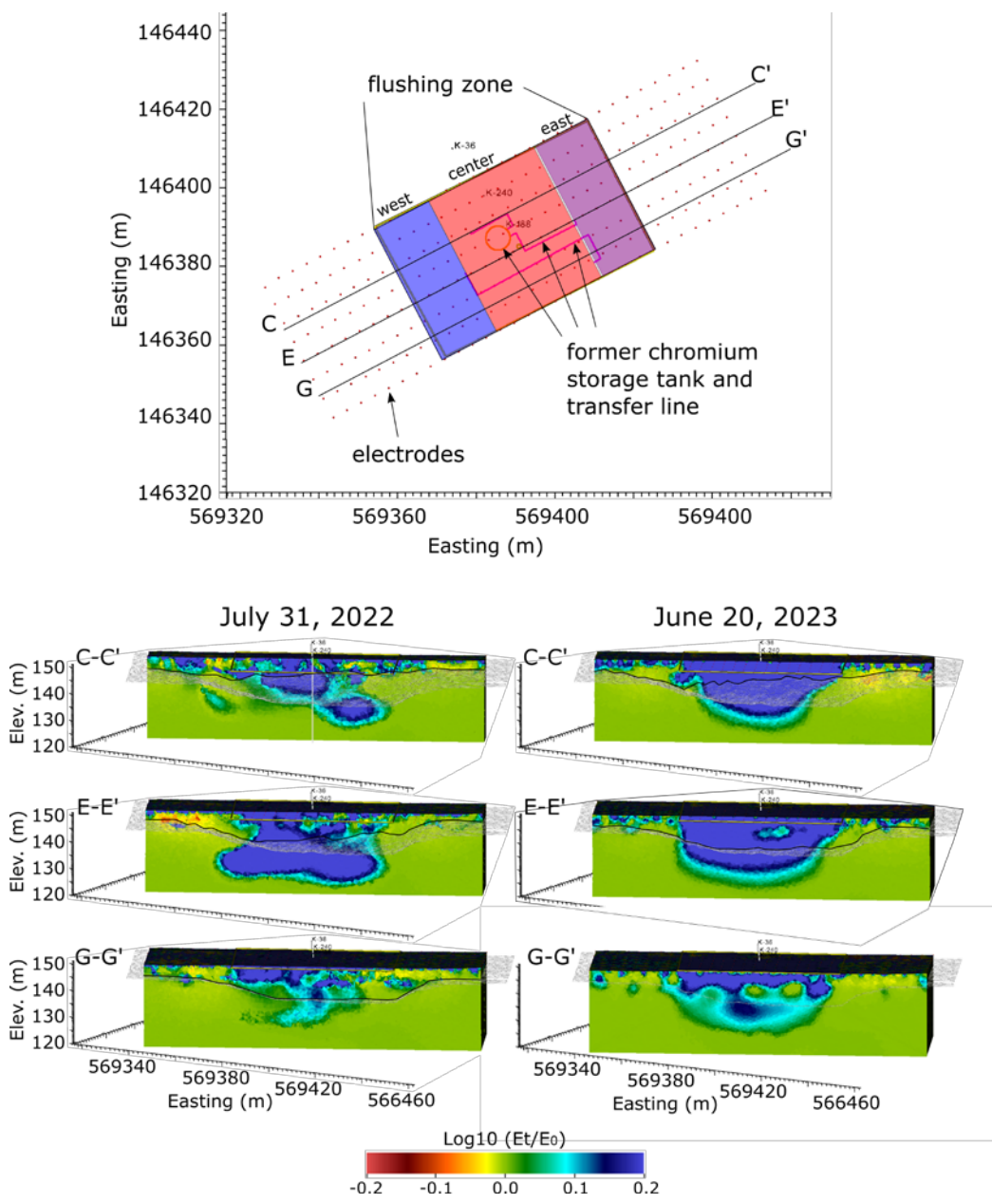


Figure S.1. Example time-lapse ERT images showing the maximum distribution of flush water (blue areas) in three cross-sections for the 2022 and 2023 100-KE soil flushing campaigns. Non-uniform flush water distribution is caused by subsurface heterogeneity. Flush water application rates were higher in 2023 than in 2022, resulting in more uniform flush water distribution throughout the targeted flushing zone.

## Acronyms and Abbreviations

BEC	bulk electrical conductivity
Cr(VI)	hexavalent chromium
ERT	electrical resistivity tomography
gpm	gallons per minute
lpm	liters per minute

## Contents

Summary .....	ii
Acronyms and Abbreviations .....	iv
1.0 Introduction.....	1
2.0 100-KE Soil Flushing Site and ERT Monitoring Array .....	3
3.0 Flush Water Application .....	7
4.0 ERT Data Collection and Processing.....	10
5.0 ERT Results Presentation Format .....	11
6.0 2022 ERT Imaging Summary and Interpretation.....	13
7.0 2023 Imaging Summary and Interpretation .....	22
8.0 Discussion and Conclusion.....	34
9.0 References.....	35
Appendix A – ERT Methods .....	A.1

## Figures

Figure 1.	Historical images of the 100-K Area, where past operations resulted in unplanned releases from the sodium dichromate storage tank located in the K-East contaminated vadose zone soils that presently act as a source zone for groundwater Cr(VI) contamination.....	3
Figure 2.	(top) Aerial view of the excavation pit constructed to removed Cr(VI)-contaminated sediments from the vadose zone. (bottom) Aerial of the soil flushing zone super-imposed on the backfilled excavation pit. ....	4
Figure 3.	Location of surface ERT electrode lines (black dots) installed over the soil flushing zone. The lateral extent of the array, which impacts imaging depth, was limited by the building foundation located at the eastern margin of the array. ....	5
Figure 4.	(top) Oblique view of the boundary between the pit backfill and the Hanford formation. (bottom) Cross-section showing the approximate position of the water table (blue inverted triangle), the Ringold Formation, the Hanford-Ringold formation contact, and the contact between the Hanford formation and pit backfill. ....	6
Figure 5.	A) Flush water application zones. B) 2022 total and zonal flush water application rates. C) Nominal 2023 total and zonal flush water applications rates.....	8
Figure 6.	(left) Photograph taken during the first week of soil flushing in 2022, highlighting flush water distribution lines. (right) Photograph highlighting the ERT electrode array (white boxes connected by cables) .....	9
Figure 7.	Screen shot of the interactive website enabling near real-time inspection of ERT imaging results.....	10
Figure 8.	Locations of cross-sections used to present ERT imaging results. ....	11
Figure 9.	Timeline and dates of 2022 ERT images with respect to flush water application rates.....	13

Figure 10. 2022 baseline ERT image collected on June 19, 2022. .... 14

Figure 11. Change in BEC on July 14, 2022, after several days of flushing at a total flush rate of approximately 303 lpm (80 gpm). .... 15

Figure 12. ERT image from July 25, 2022, after 11 days rest from soil flushing ..... 16

Figure 13. ERT image from July 31, 2022, after approximately 7 days of flushing in the central and western flush zones. .... 17

Figure 14. ERT image from August 12, 2022, after approximately 2 weeks of continuous flushing in the center flush zone and 1 week of continuous flushing in the eastern flush zone. .... 18

Figure 15. ERT image from August 19, 2022. .... 19

Figure 16. ERT image from August 26, 2022. .... 20

Figure 17. ERT image from November 30, 2022. .... 21

Figure 18. Times and dates of 2023 ERT images presented in section and corresponding flush water application rates. .... 22

Figure 19. 2023 baseline ERT image from March 30, 2023. .... 23

Figure 20. ERT image from April 8, 2023, after 1 week of soil flushing. .... 24

Figure 21. ERT image from April 15, 2023, after 2 weeks of soils flushing. .... 25

Figure 22. ERT image from April 27, 2023, after 3 weeks of soil flushing. .... 26

Figure 23. ERT image from April 29, 2023, after 4 weeks of soil flushing. .... 27

Figure 24. ERT image from May 6, 2023, after 5 weeks of soil flushing. .... 28

Figure 25. ERT image collected on May 15, 2023, after 6 weeks of soil flushing. .... 29

Figure 26. ERT image from May 22, 2023, after 7 weeks of soil flushing. .... 30

Figure 27. ERT image from May 29, 2023, after 8 weeks of soil flushing. .... 31

Figure 28. ERT image from June 20, 2023, after 11 weeks of soil flushing. .... 32

Figure 29. ERT image from June 26, 2023, 4 days after the end of soil flushing. .... 33

## 1.0 Introduction

Former operations in the 100-KE Area at the Hanford Site resulted in vadose zone hexavalent chromium [Cr(VI)] that provides a source of groundwater contamination. Contaminated groundwater is currently being hydraulically captured, removed, and transported to a pump-and-treat (P&T) facility through a series of extraction wells. Although these current mitigation procedures are protective of the Columbia River, vadose zone soils within the 100-KE Area are expected to provide a continued source of groundwater Cr(VI) that may prevent site closure for decades.

Previous efforts to remediate Cr(VI)-contaminated soils involved excavation and removal, whereby contaminated vadose soils were identified by direct sampling and removed for offsite treatment and storage. Excavation and treatment resulted in an excavation pit with required side slopes that could no longer be feasibly maintained once the pit reached a certain depth. The pit was backfilled, and *in situ* soil flushing was identified as a viable alternative to remediate contaminated soils beneath the pit boundary.

*In situ* soil flushing was used at the 100-KE Area to accelerate the removal of the Cr(VI) source zone. Soil flushing works by applying a continuous stream of clean water at the surface and allowing it to percolate to the water table. As the water migrates downward through contaminated soil, it transports the Cr(VI) from contaminated vadose zone soils to the groundwater, where it is removed through P&T extraction. The efficacy of soil flushing is directly related to the volume of water that infiltrates through contaminated soils (Szecsody et al. 2022, 2023). In practice, it is infeasible to comprehensively monitor which regions of the vadose zone are being infiltrated through direct sampling of pore water. Consequently, there can be significant uncertainty concerning how well a given region of the subsurface has been treated, especially if hydrogeologic conditions and application rates favor the development of unstable flows and preferred flow pathways through the vadose zone (Jarvis et al. 2016).

Time-lapse electrical resistivity tomography (ERT) imaging is a method of remotely imaging spatial and temporal changes in the bulk electrical conductivity (BEC) of the subsurface. Because BEC is governed in part by soil saturation, 3D time-lapse ERT can be an effective tool for monitoring when and where the vadose zone is impacted by flush water. ERT works by injecting electrical currents and measuring electrical potentials (i.e., voltages) on an array of electrodes installed (in this case) along the ground surface. ERT data is then numerically processed to produce an imperfectly resolved image of subsurface BEC. In monitoring applications, ERT data is collected on a repeating schedule and processed to produce images of changes in BEC over time. During soil flushing, increases in BEC with respect to background conditions are diagnostic of increased soil moisture. Time-lapse images of increases in BEC may therefore be interpreted to diagnose when and where flush water has impacted a given region of the vadose zone.

This report presents the results and interpretations of time-lapse ERT images collected during two separate soil flushing campaigns conducted in the 100-KE area in 2022 and 2023. Flushing operations in 2022 began with a weeks-long testing period characterized by intermittent flushing that enabled both the saturating and desaturated regions of target zone to be imaged. The testing period was followed by a months-long period of continuous flushing at a low flush water application rate in comparison to 2023. Flushing operations in 2023 ran continuously for 11 weeks, with weekly increases in application rate for the first 8 weeks. Maximum sustained flush water application rates in 2023 were approximately twice the 2022 application rates. ERT imaging results show generally that subsurface heterogeneity had a significant impact on flush water migration through the vadose zone in 2022 and 2023. Native soils beneath the bottom of the pit boundary appear to have received the highest volumes of flush water, while native soils beneath shallow sections of the pit boundary received the lowest volumes. In addition, the

larger flushing rates applied in 2023 significantly improved flush water distribution throughout the target zone in comparison to 2022.

The remainder of this report is organized as follows: Section 2.0 discusses the 100-KE soil flushing zone and ERT array, Section 3.0 describes how flow water was applied at the surface in both the 2022 and 2023 flushing campaigns, Section 4.0 describes aspects of the ERT data collection and processing, Section 5.0 describes how the ERT images are presented in Sections 6.0 (2022) and 7.0 (2023). Section 8.0 provides concluding observations and remarks. Appendix A provides information on ERT measurements and imaging resolution.

## 2.0 100-KE Soil Flushing Site and ERT Monitoring Array

Hanford's 100-KE and 100-KW areas housed two plutonium production reactors and support facilities, situated adjacent to the Columbia River on the northeastern margin of the site. Figure 1 shows three historical images of the Hanford 100-K Area. The 100-KE Area includes the K-East reactor and supporting facilities, including a sodium dichromate storage tank and transport piping as shown in the annotated areas in Figure 1, 1964 and 2017 images. Sodium dichromate was used to inhibit piping corrosion. During operations, releases of sodium dichromate occurred in the K-East Area, contaminating vadose zone sediments and creating a continuing source zone of Cr(VI) to the groundwater.

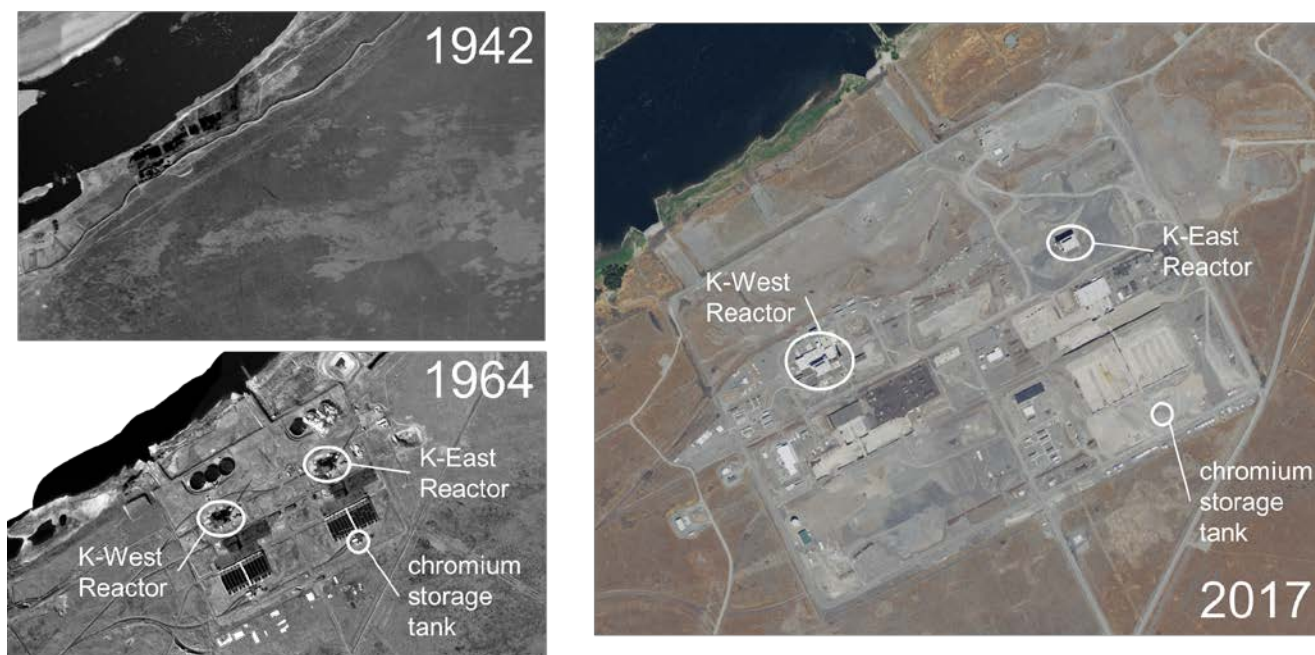


Figure 1. Historical images of the 100-K Area, where past operations resulted in unplanned releases from the sodium dichromate storage tank located in the K-East contaminated vadose zone soils that presently act as a source zone for groundwater Cr(VI) contamination.

Initial efforts to remediate Cr(VI)-contaminated soils involved excavation and removal. Excavation involved testing soils at the bottom of the excavation pit for Cr(VI) and excavating where contaminated soils were found. Maintaining side-slopes required for geotechnical stability became infeasible after the pit reached approximately 8 m below the ground surface, and the pit was re-filled to grade with clean backfill.

After the excavation pit was backfilled, soil flushing was chosen to remediate contaminated soils remaining beneath the pit boundary. Figure 2 (top) shows an aerial image of the pit taken near the end of excavation operations. Figure 2 (bottom) shows the flushing zone boundary superimposed on an aerial image of the backfill excavation pit.

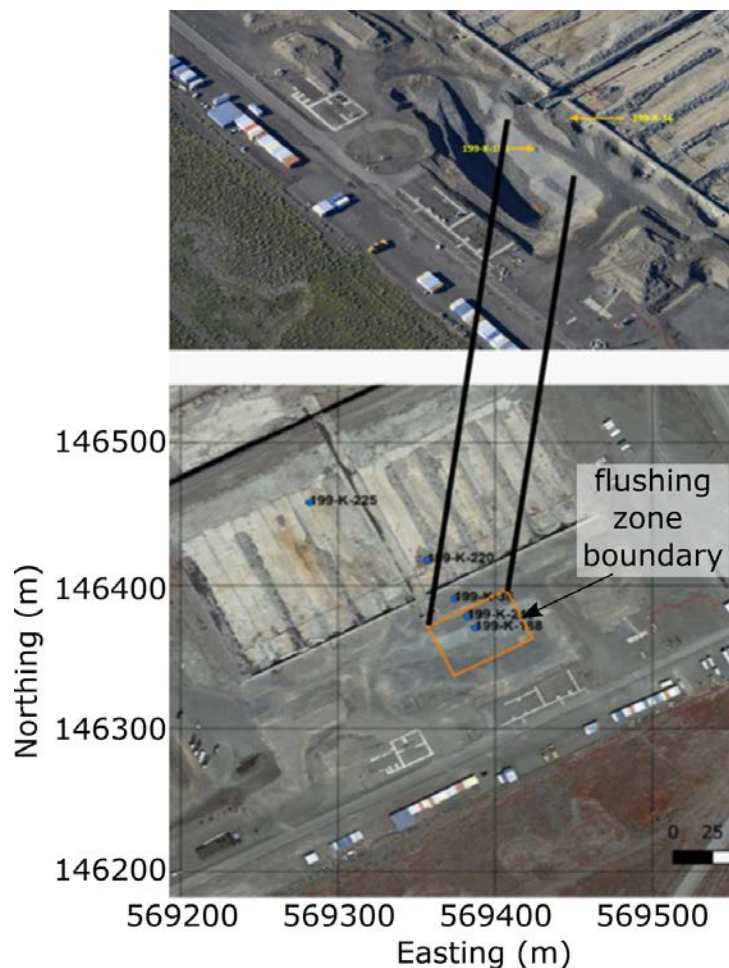


Figure 2. (top) Aerial view of the excavation pit constructed to removed Cr(VI)-contaminated sediments from the vadose zone. (bottom) Aerial of the soil flushing zone super-imposed on the backfilled excavation pit.

Soil flushing was implemented by applying clean flush water at the ground surface using an array of dispersion hoses distributed within the flush zone. To monitor the migration of flush water through the vadose zone, a surface-based ERT electrode array was installed over the flush zone as shown in Figure 3. Array dimensions and electrode placement were chosen based on the ERT feasibility and performance simulations reported in Johnson et al. (2020). The array consisted of 8 lines of 32 electrodes each, with 4-m spacing between electrodes and 5.4-m spacing between lines. ERT imaging depth is determined in large part by the length of the array. In this case, the line lengths were limited by the building foundation located on the eastern margin of the array. Consequently, imaging depth was limited to approximately 20 m below the current ground surface elevation, or approximately 10 m beneath the bottom of the pit boundary.

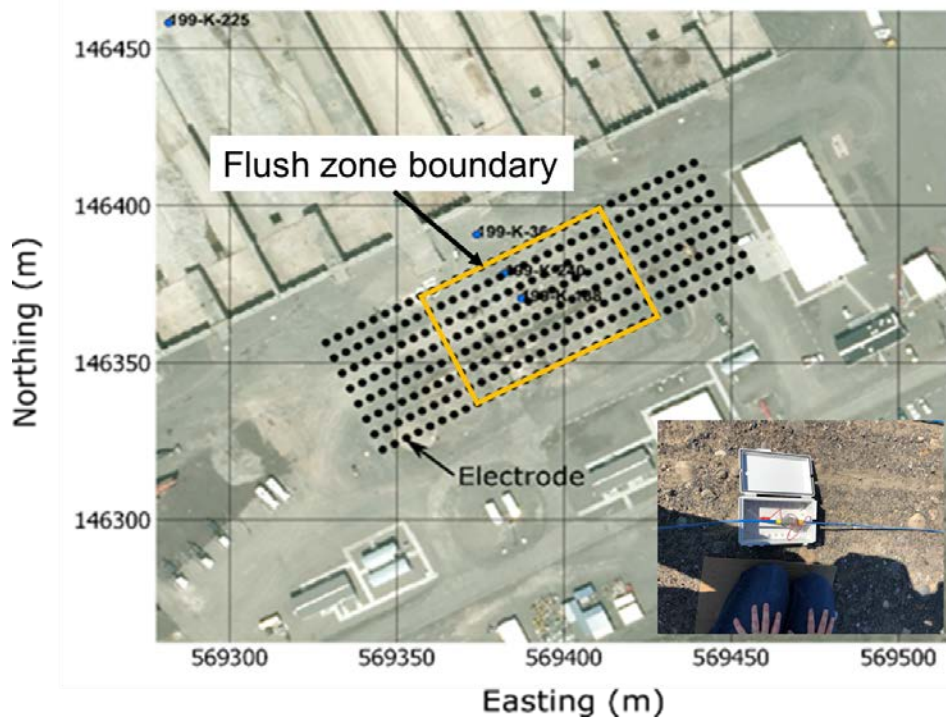


Figure 3. Location of surface ERT electrode lines (black dots) installed over the soil flushing zone. The lateral extent of the array, which impacts imaging depth, was limited by the building foundation located at the eastern margin of the array.

For perspective, Figure 4 (top) shows an oblique 3D view of the pit backfill boundary, flush zone boundary, electrode positions, extraction well positions, and the location of historical Cr(VI) handling infrastructure (i.e., tanks and piping systems) suspected of releasing Cr(VI) during site operations. Figure 4 (bottom) shows a vertical cross-section oriented perpendicular to the long axis of the infiltration zone, including the locations of the undisturbed Hanford and Ringold formations as interpreted from geologic logs. The interface between the bottom of the pit backfill and the top of the Hanford formation is located at least 2 m below the ground surface at its shallowest point within the soil flushing zone, and ~10 m at its deepest point. Consequently, all flush water applied at the surface migrates through a section of backfill material before reaching the Hanford formation interface. Furthermore, the contact between backfill materials and the Hanford formation angles downward toward the bottom of the pit at the pit margins, which is an important feature when interpreting the ERT imaging results. With respect to Figure 4 (bottom), ERT imaging resolution extends to an elevation of ~130 m, leaving the 10-m interval from the water table (~120 m elevation) to 130 m in elevation unresolved.

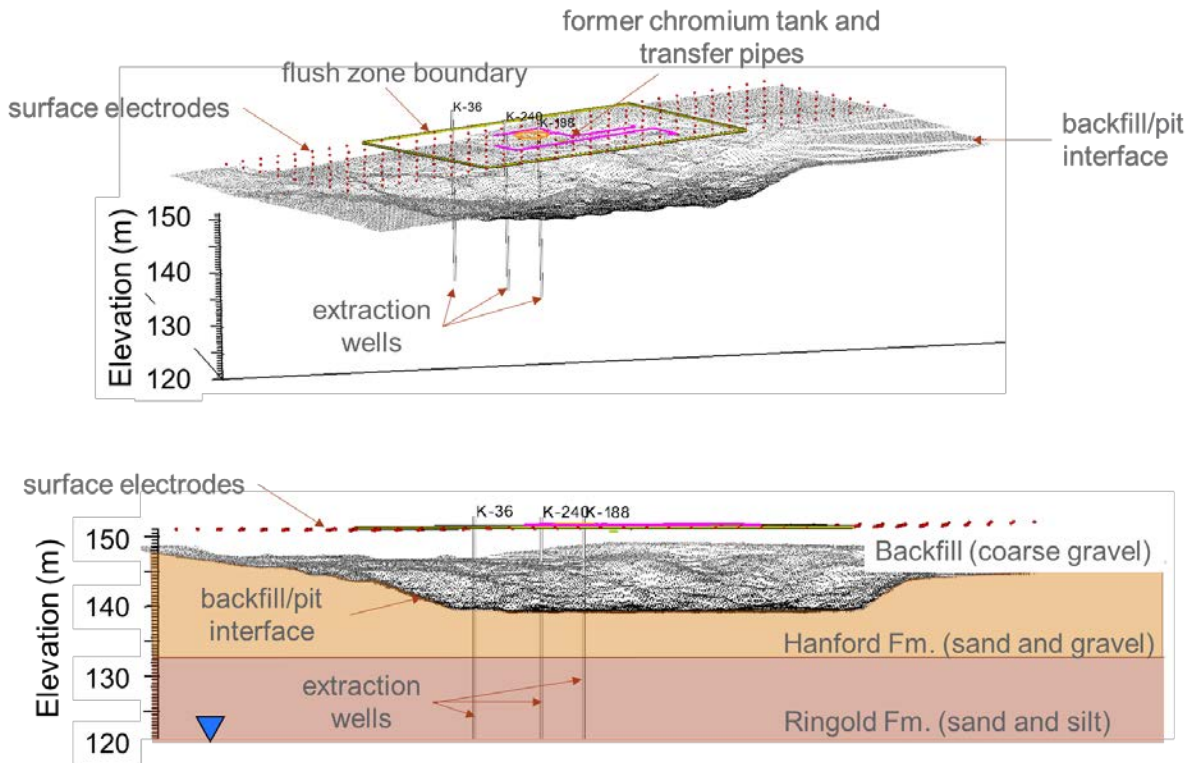


Figure 4. (top) Oblique view of the boundary between the pit backfill and the Hanford formation. (bottom) Cross-section showing the approximate position of the water table (blue inverted triangle), the Ringold Formation, the Hanford-Ringold formation contact, and the contact between the Hanford formation and pit backfill.

### 3.0 Flush Water Application

Flush water was applied in three different zones (west, center, and east) within the infiltration gallery, as shown in Figure 5A. Application rates in 2022 for each zone are shown in Figure 5B. In 2022, system testing began on June 21 and proceeded with intermittent flushing until July 25. From July 25 to November 8, flushing proceeded continuously in the center zone at a rate of between 87-145 lpm (22-38 gpm). During the same period, flush water application switched approximately weekly between the west and east flush zones, with flush water being applied at 45-82 lpm (12-22 gpm). The average total application rate from July 25 to November 8 was 172 lpm (45 gpm). Flushing operations were halted on November 8 and resumed in April of 2023.

In 2023, flush water application began on April 3 at a rate of 142 lpm (37.5 gpm) in the center zone and 47.3 lpm (12.5 gpm) in the west zone. As shown in Figure 5C, application rates increased weekly within the center zone for the first 3 weeks and switched weekly between the west and east zones. On April 25, flush water began to be applied continuously throughout the flush zone at a rate of 151 lpm (40 gpm) in the center zone and 76 lpm (20 gpm) in both the east and west zones, for a total application rate of 303 lpm (80 gpm). From there, application rates were increased weekly, reaching a sustained maximum of 265 lpm (70 gpm) in the center zone and 95 lpm (25 gpm) in both the west and east zones on May 24, for a total of 454 lpm (120 gpm). Those rates were sustained until June 22, 2023, when flushing operations were halted.

Figure 6 shows two photographs of the soil flushing system operating during the first week of flushing in 2022. Flush water application lines are shown in Figure 6 (left), and the ERT array (i.e., white boxes connected by cables) is shown in Figure 6 (right). Of note is the distribution of shallow surface ponding shown in Figure 6 (right), caused by slight variations in surface topography. Regions of ponding may have facilitated the development of preferred vadose flow-paths within the backfill soils that are evident in the forthcoming ERT images.

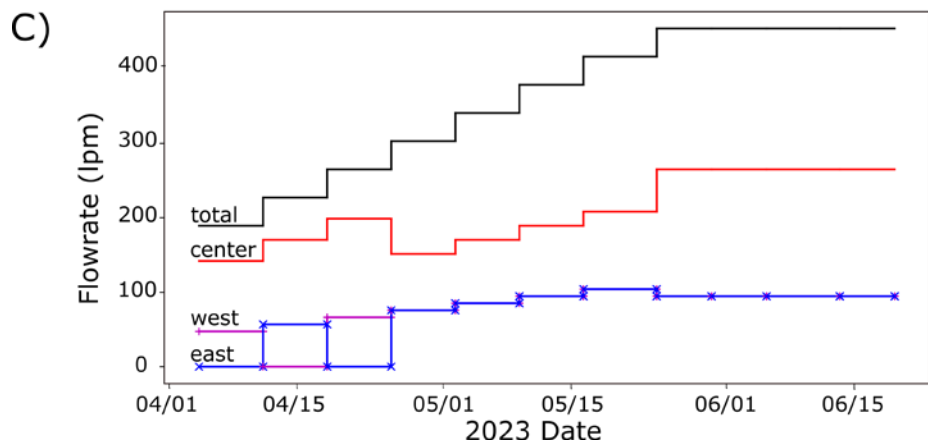
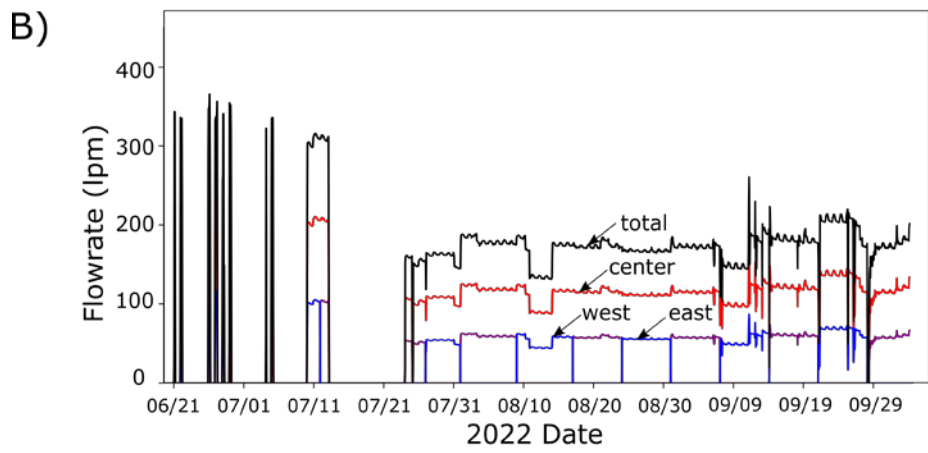
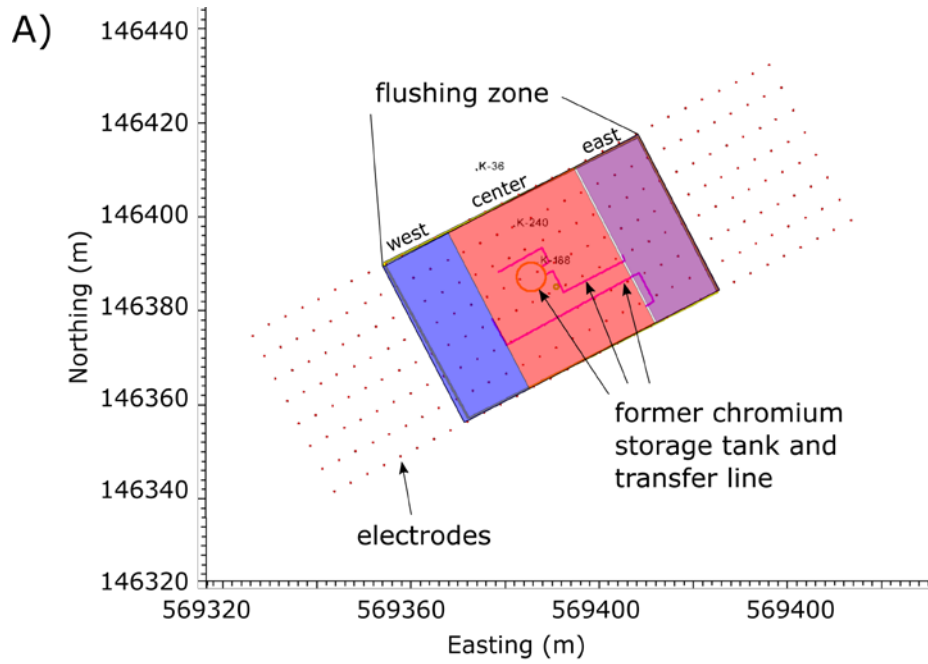


Figure 5. A) Flush water application zones. B) 2022 total and zonal flush water application rates. C) Nominal 2023 total and zonal flush water applications rates.



Figure 6. (left) Photograph taken during the first week of soil flushing in 2022, highlighting flush water distribution lines. (right) Photograph highlighting the ERT electrode array (white boxes connected by cables)

## 4.0 ERT Data Collection and Processing

ERT surveys were collected nominally every 2 hours before, during, and after the 2022 and 2023 soil flushing campaigns. Data were collected using a commercial eight-channel data collection system, which allows potential measurements to be collected between eight electrode pairs per current injection pair. In total, 4730 Wenner, in-line and cross-line four-electrode dipole-dipole measurements were collected per survey, with offsets designed to maximize both shallow and deep resolution. Each survey required 52 minutes to complete. To assess noise conditions, ERT surveys were collected every 2 hours for 3 days prior to the application of flush water in 2022. Each of the 4730 time-series were analyzed for noise conditions, and measurements with standard deviations greater than 10% of the mean were removed from the survey, resulting in a loss of 22 measurements. Overall, the ERT data were of high quality throughout both soil flushing campaigns. The remaining 4708 measurements collected at each survey time were processed to produce time-lapse ERT images. Additional information regarding ERT data collection and resolution is provided in Appendix A.

Upon completion, data collected during each survey were transferred to offsite high-performance computing resources for quality assessment, processing, and archival. Data were inverted in parallel using 67 central processing units, requiring 5 to 15 minutes for completion. To reduce inversion artifacts from metallic infrastructure, the metallic extraction well (K-240) casing was explicitly modeled using the method of Johnson and Wellman (2015). However, artifact removal cannot account for the decrease in resolution caused by buried metallic structures. As will be shown, decreased resolution is evident in the ERT images near the K-240 well.

Each ERT image was posted on a secured, interactive website that enabled online visualization of the results as they became available. A screen shot of the website is shown in Figure 7. Results posted to the website were preliminary and may not be identical to the results presented in this report.

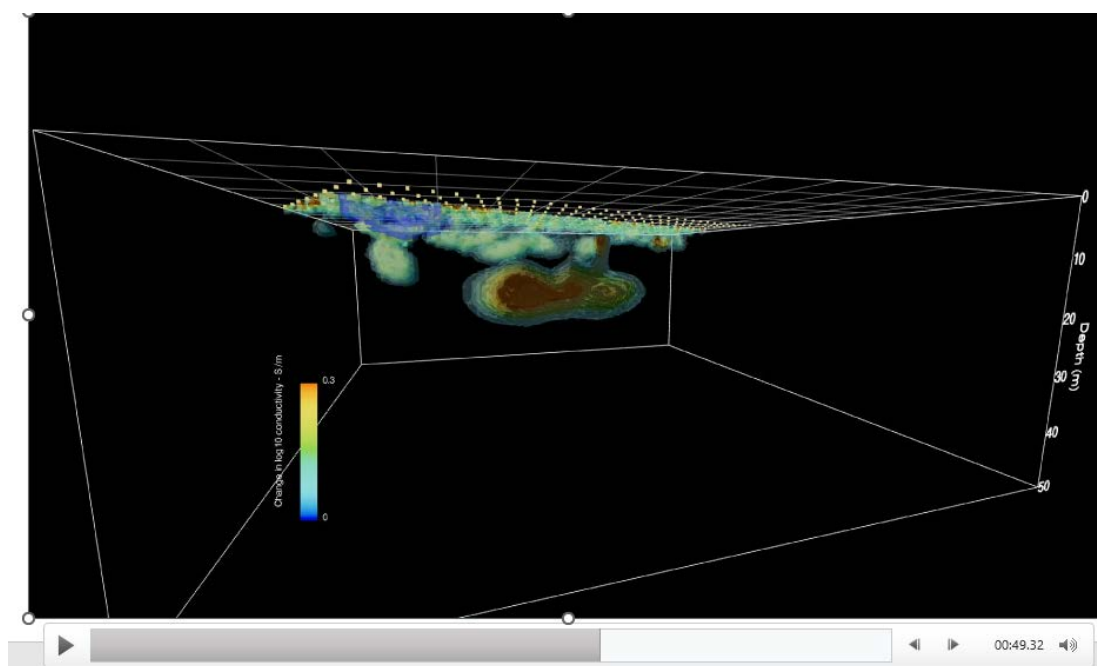


Figure 7. Screen shot of the interactive website enabling near real-time inspection of ERT imaging results.

## 5.0 ERT Results Presentation Format

The following sections present ERT images at select times in a series of eight cross-sections at the locations shown in Figure 8 (top). Each cross-section is aligned parallel to the long axis of the flushing gallery and electrode line. Cross-section spacing is meant to be small enough facilitate understanding of the 3D distribution of flush water at a given time, by visualizing (for example) the image progression from cross-section A to cross-section H.

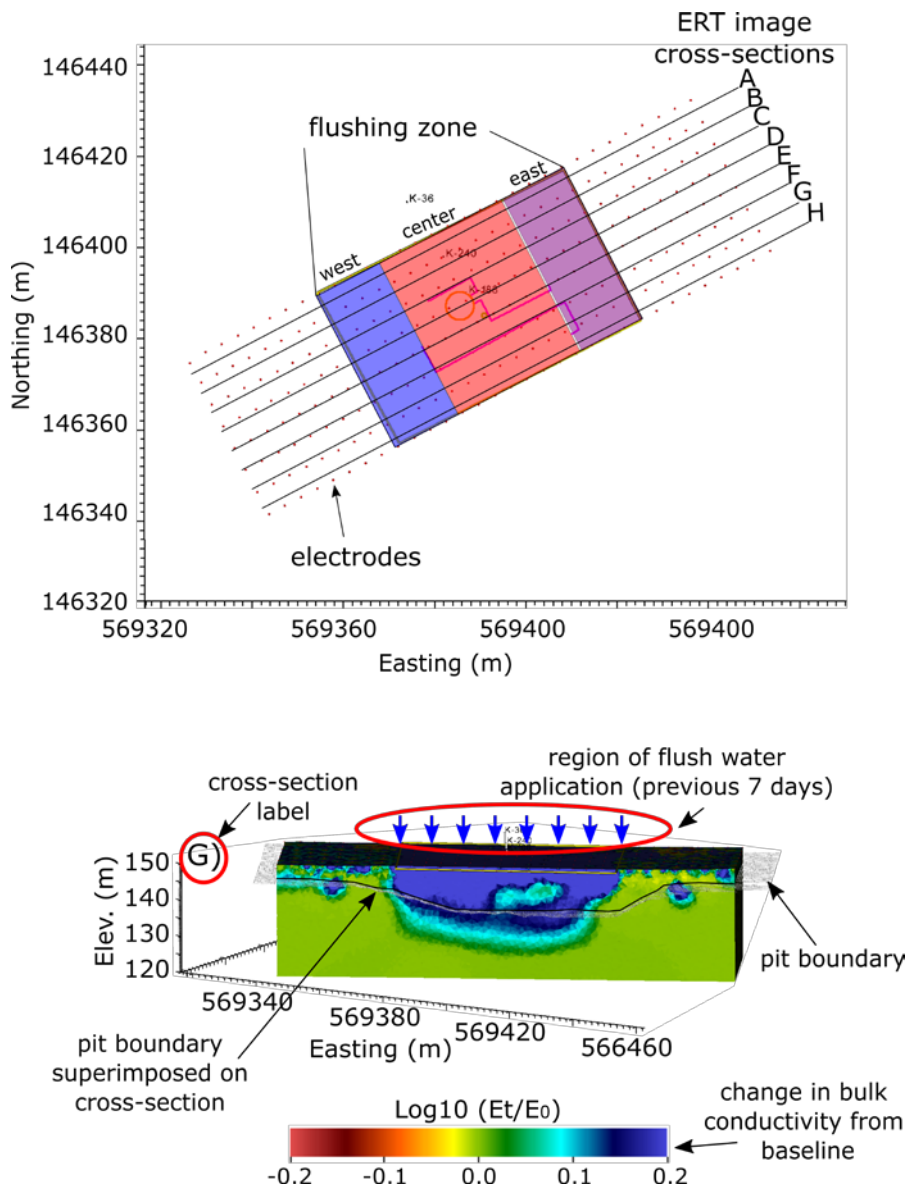


Figure 8. Locations of cross-sections used to present ERT imaging results.

An example cross-section is shown in Figure 8 (bottom), cross-section G in this case. Each cross-section will include the cross-section label, the 3D pit boundary (dotted surface), and the intersection of the pit boundary and the cross-section (black line). The pit boundary is shown in each image because it has a significant influence on the distribution of flush water and marks the interface between backfill materials and the Hanford formation. Images presented were generally acquired after 7 days of continuously

flushing in a region. The region where flush water was applied during the 7 days prior to a given ERT image is shown by blue arrows. The color of the cross-section indicates the change in BEC from baseline conditions, which were imaged before flush water was applied in both 2022 and 2023. The blue end of the color scale represents an increase in BEC (i.e., associated with an increase in saturation), and the red end represents a decrease in BEC from baseline conditions.

## 6.0 2022 ERT Imaging Summary and Interpretation

Figure 9 shows the timeline and dates of ERT images presented in this section. Each image time was chosen to highlight flush water dynamics due to changing application rates and locations, and the effects vadose zone heterogeneity. The flushing campaign images for 2022 begin in June with a pre-flushing (baseline) image (Figure 10) and finish in November with a post-flushing image (Figure 17).

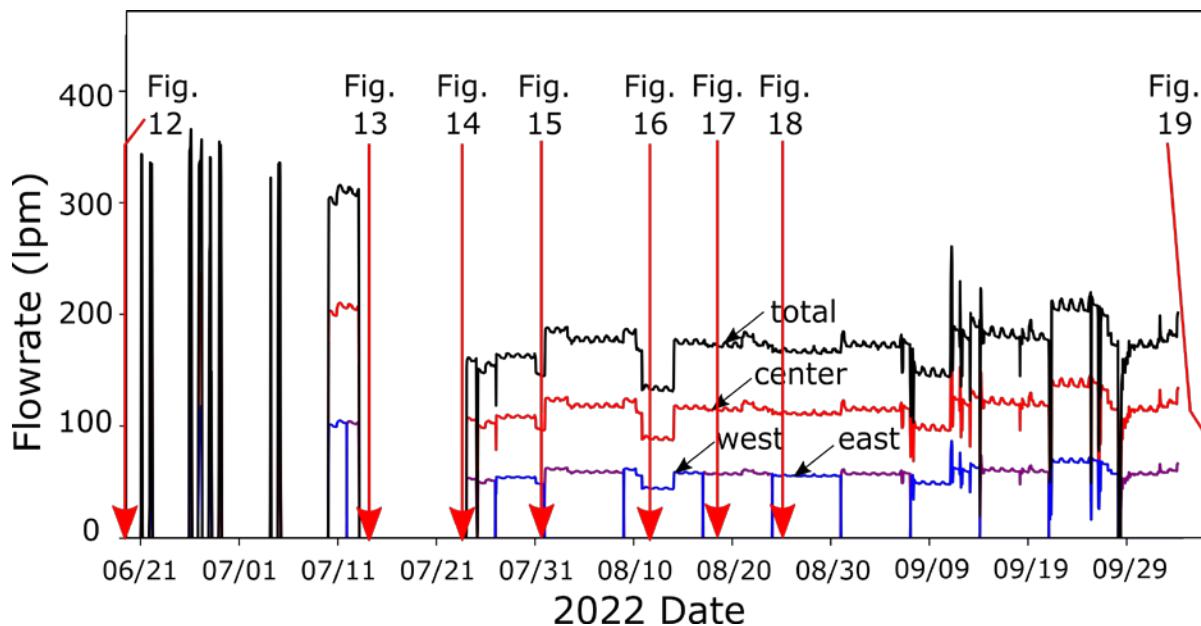


Figure 9. Timeline and dates of 2022 ERT images with respect to flush water application rates.

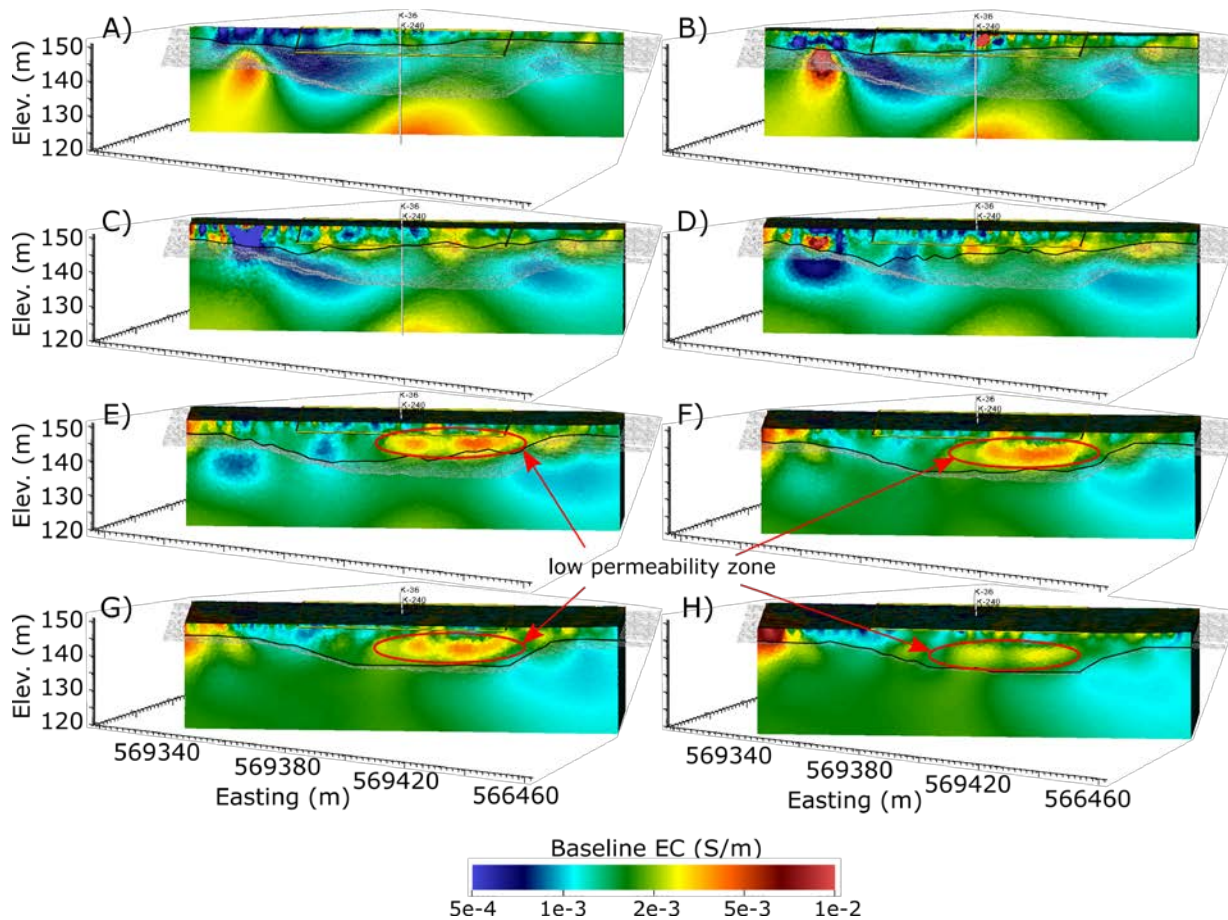


Figure 10. 2022 baseline ERT image collected on June 19, 2022.

Figure 10 shows the 2022 baseline ERT image collected 2 days prior to the first application of flush water on June 21, 2022. The baseline image is subtracted from every subsequent image collected during soil flushing to reveal increases in BEC associated with increases in soil saturation over time. Spatial variations in BEC within the baseline image may be caused by variations in porosity, soil saturation, pore fluid conductivity, or soil texture. Absolute BEC variations cannot be uniquely attributed to any single property without supporting information. However, transient changes in BEC can often be uniquely attributed to a single process such as the increase in saturation caused by soil flushing in this case. Figure 10 highlights an elevated region of baseline BEC within the pit backfill, which is inferred to be a relatively low-permeability zone based on flush water flow behavior evident in the forthcoming time-lapse images, acting as a barrier for downward migration of flush water.

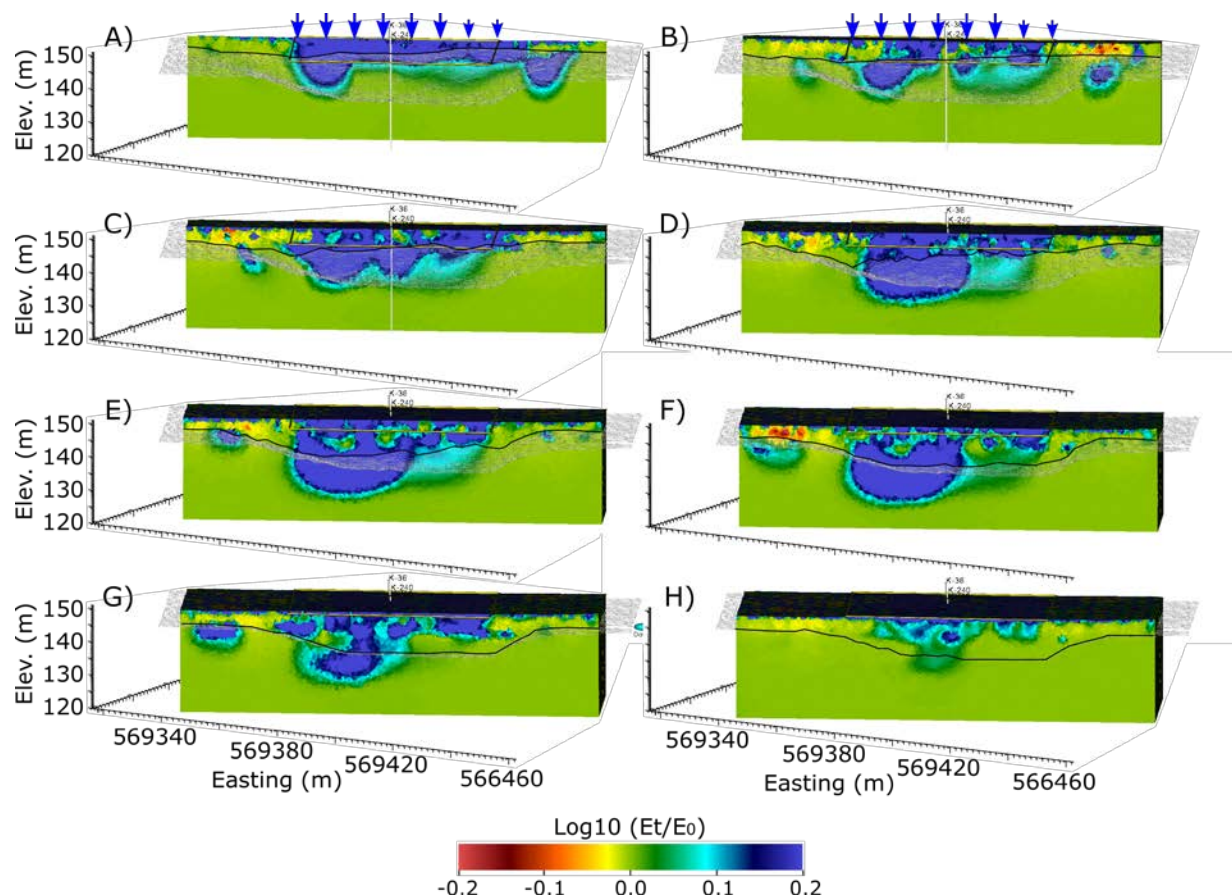


Figure 11. Change in BEC on July 14, 2022, after several days of flushing at a total flush rate of approximately 303 lpm (80 gpm).

Figure 11 shows the change in BEC from baseline conditions on July 14, 2022, after several days of relatively high flowrate flushing. For the preceding 3 days, flush water was applied continuously to the center zone at ~200 lpm (53 gpm), and to the west zone at ~100 lpm (26 gpm) for 2 days, and then to the east zone at the same flowrate for 1 day (Figure 9). Vertical migration of flush water gradually increases from cross-sections A-D as the pit boundary gets deeper, and is deepest in cross-sections E and F, which intersect the bottom of the pit boundary. These results suggest that in sections A-F, flush water migrates downward more quickly through the backfill sediments than the Hanford formation. Flush water also appears to migrate laterally along the pit boundary, particularly in cross-section A, where the pit boundary is nearest to the surface. Flush water is clearly impeded at the pit boundary in cross-sections A and B, suggesting that some flush water is migrating down-slope along the pit boundary toward cross-section C.

In cross-sections E-G, there appears to be a vertical flow barrier corresponding to the position of the high BEC zone highlighted in the baseline image (Figure 10). Of all the cross-sections, H exhibits the least amount of vertical migration through the backfill materials, suggesting that (1) backfill materials exhibit relatively low permeability on the southern boundary of the flush zone, or (2) flush water is not evenly applied at the surface, with less water applied at the southern boundary (cross-section H). As will be shown, these observations are consistent with imaging results collected throughout the 2022 and 2023 soil flushing campaigns.

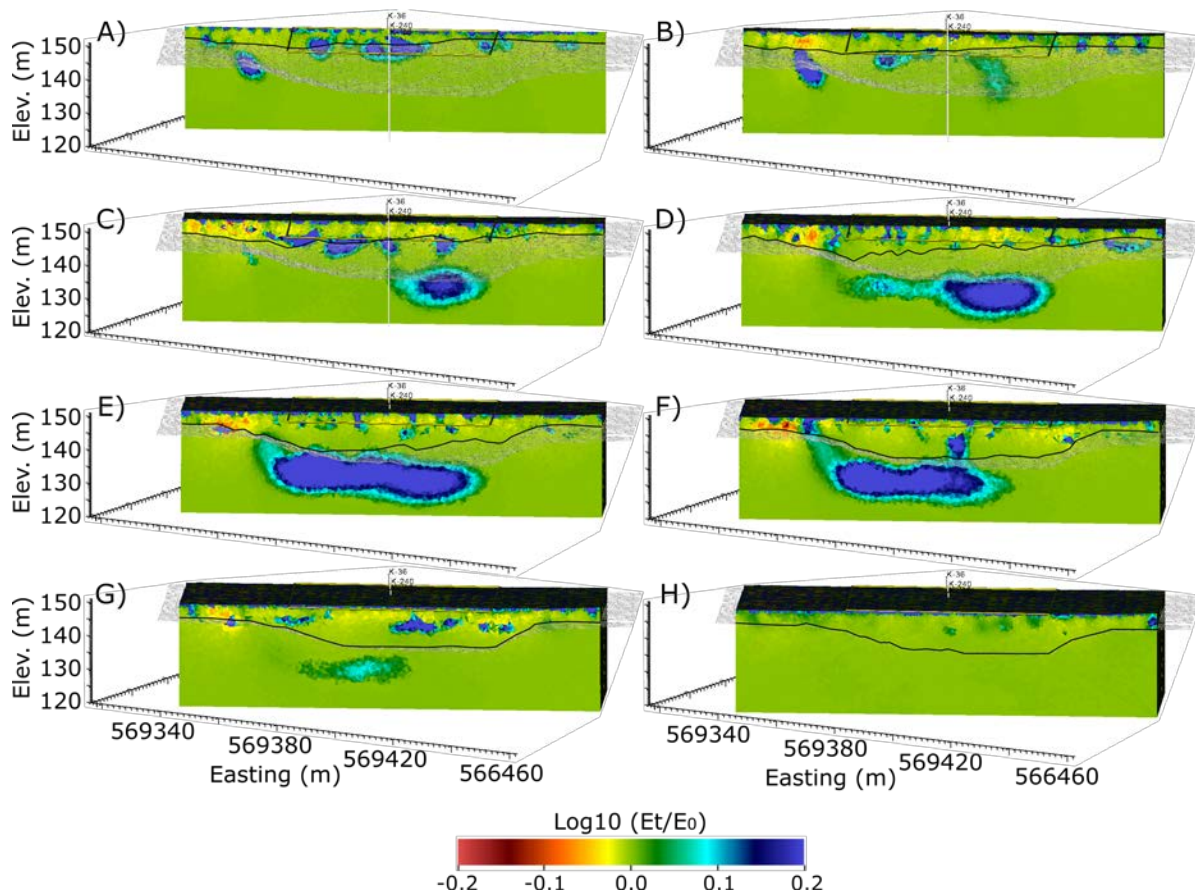


Figure 12. ERT image from July 25, 2022, after 11 days rest from soil flushing.

Figure 12 shows the change in BEC on July 25, 2022, after 11 days of rest from soil flushing (Figure 9). Flush water has largely drained from the backfill materials, leaving a plume of flush water in the Hanford formation only beneath the deepest portions of the pit boundary (cross-sections C-E). The lack of flush water in the Hanford formation beneath cross-sections A and B suggests that flush water transported along the pit interface from cross-sections A to B to C toward the bottom of the pit before migrating into the Hanford formation. Note also that the flush water within the Hanford formation in cross-sections E and F is elongated in comparison to July 14, suggesting that either (1) additional flush water migrated to E and F after flush water surface application ceased on July 14, or (2) flush water migrated laterally within the Hanford formation after July 14. The first possibility is consistent with behavior that would be expected from relatively high permeability in the backfill material compared to the Hanford formation, and the consequent redirection of flush water along the pit boundary toward the bottom of the pit.

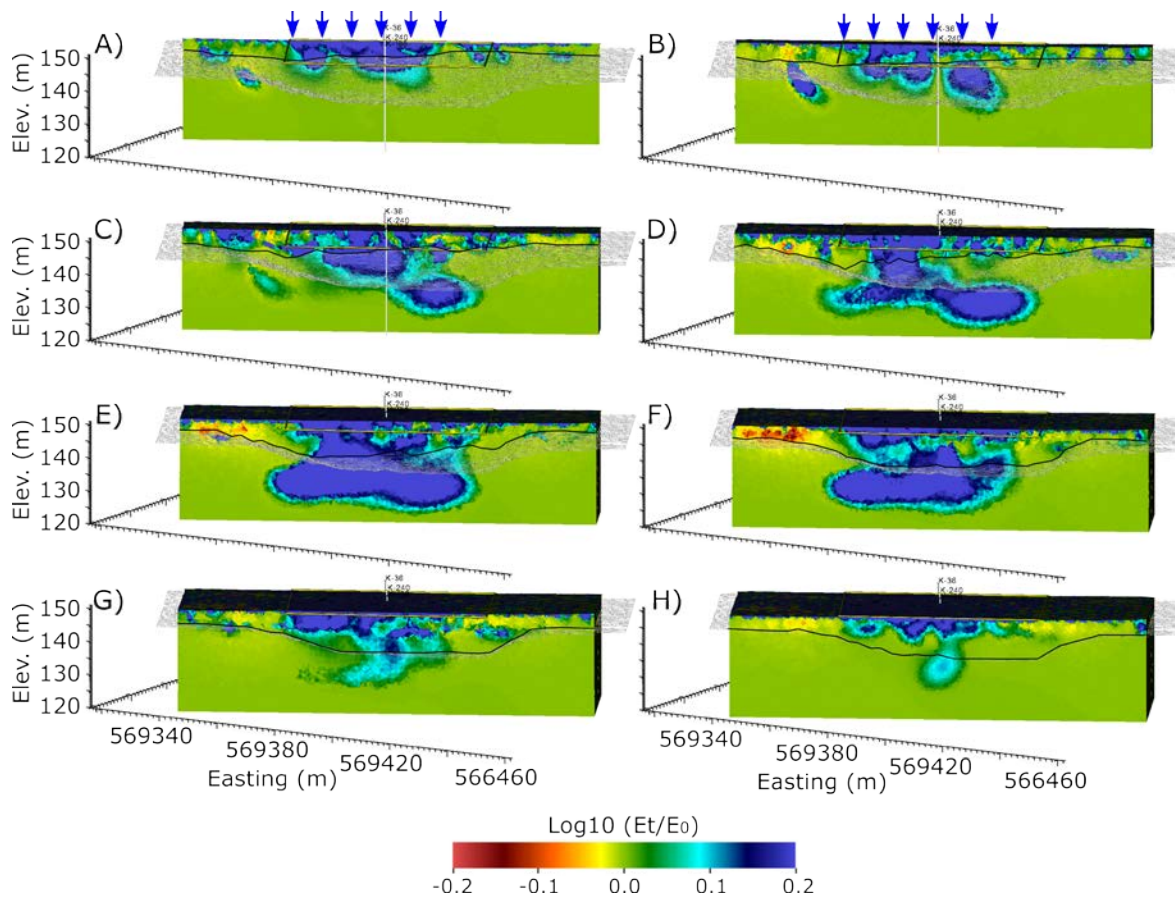


Figure 13. ERT image from July 31, 2022, after approximately 7 days of flushing in the central and western flush zones.

Figure 13 shows changes in BEC on July 31, 2022, after the first 7 days of continuous flushing in the center and western flush zones. Consistent with previous observations, the greatest amount of flush water migration into the Hanford formation occurs in cross-sections E and F, which intersect the bottom of the pit. Migration of flush water appears to be impeded by the shallow pit boundary interface in cross-sections A and B, suggesting that flush water may have been transported down-slope along the pit boundary from A to B to C, etc. Several regions of focused flow appear to develop within the pit backfill materials in cross-sections A-F, which can occur in unsaturated, high-permeability sediments (Glass et al. 1990; Jarvis et al. 2016). As will be shown in the forthcoming images, flow focusing appears to increase with time in both the backfill materials and the Hanford formation.

In comparison to the six northern cross-sections (A-F), vertical flush water migration within cross-sections G and H appears to be impeded within the backfill materials (i.e., above the pit boundary). If flush water was applied evenly at the surface, the impeded vertical flow in G and H suggest flush water must have migrated northward toward cross-section F (or southward out of the imaging zone) before moving deeper into the backfill material.

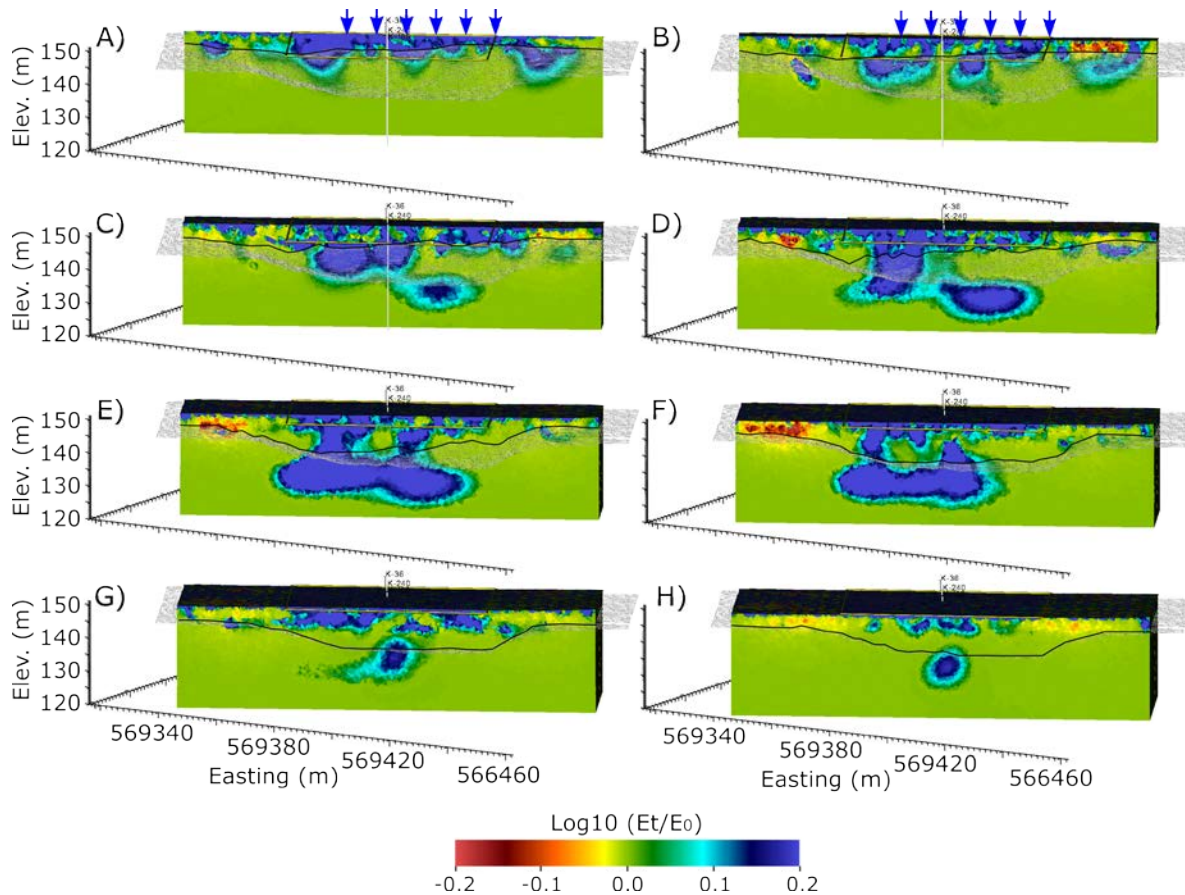


Figure 14. ERT image from August 12, 2022, after 2 weeks of continuous flushing in the center flush zone and 1 week of continuous flushing in the eastern flush zone.

Figure 14 shows changes in BEC on August 12, 2022, after 2 full weeks of continuous flushing within the center flush zone and 1 week of flushing within the eastern flush zone (Figure 9). Results are mostly consistent with the July 31 image, except that the regions impacted by flush water have contracted slightly, possibly resulting from the reduced flush water application rate experienced from approximately August 11 to 15 (Figure 9). Cross-sections G and H show flush water within the Hanford formation that is not directly connected to a vertical flow path, suggesting flush water is migrating laterally southward within the Hanford formation from F to G to H. Cross-sections B-F show non-uniform, focused flow within the backfill materials, underlain by elongated regions of flush water in the Hanford formation, which is further evidence of lateral spreading within the Hanford formation.

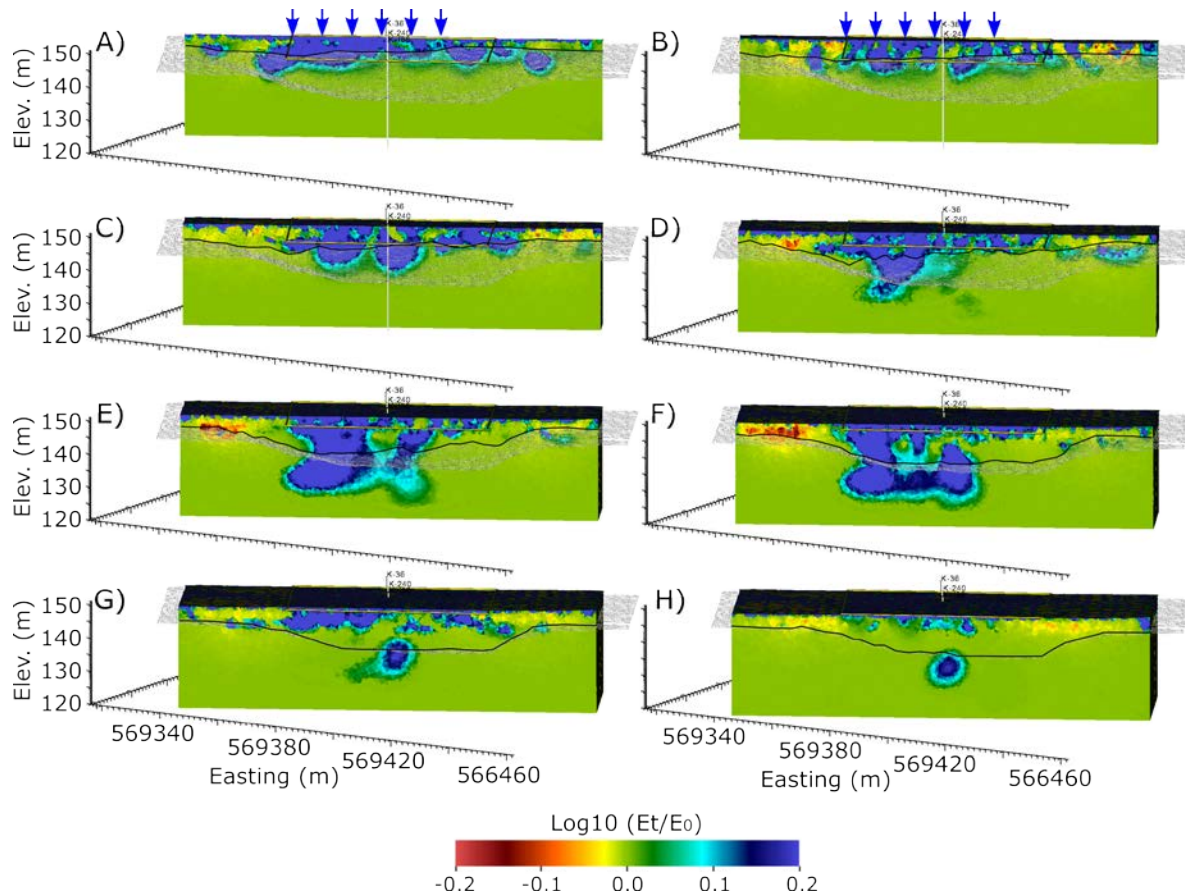


Figure 15. ERT image from August 19, 2022.

Figure 15 shows changes in BEC on August 19, 2022. The results and interpretation are like those for August 12 (Figure 14), except that regions impacted by flush water within the Hanford formation have contracted slightly. This may be caused by the continuous development of focused flow paths, possibly facilitated by weekly switches in flush water application between the east and west flush zones. Consider cross-section E, for example. On August 12 (Figure 14), when flush water was being applied to the central and eastern flush zones, flush water distribution within the Hanford formation is more extensive than on August 19, particularly in the eastern half of the Hanford formation. From cross-sections D to F, a dominant and continuous flow path appears to have developed in the western half (i.e., west of the extraction well) that extends from the backfill materials through the pit boundary and into the Hanford formation. Cross-sections A-C continue to show relatively inhibited vertical flow through the pit boundary, suggesting that some flush water is migrating along the pit boundary from A to B to C and onward toward the bottom of the pit.

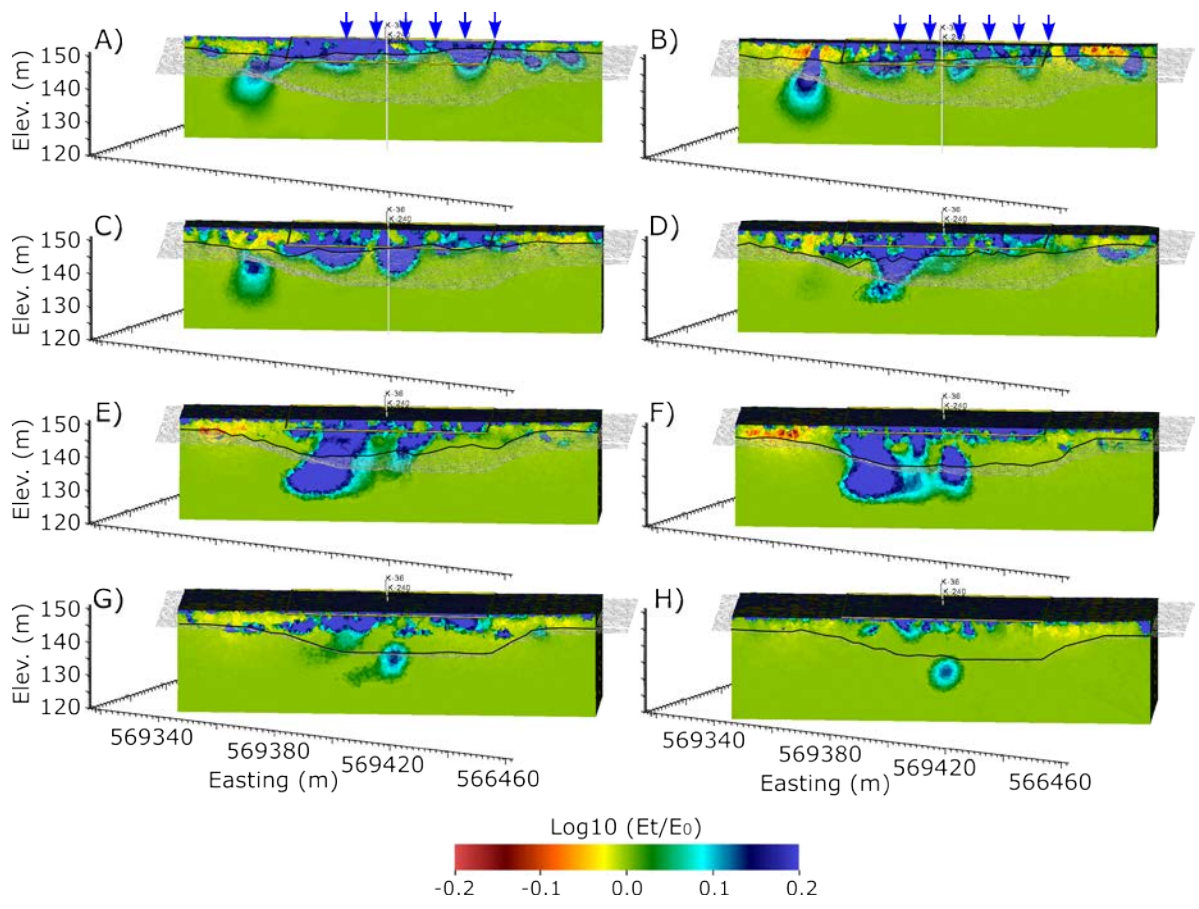


Figure 16. ERT image from August 26, 2022.

Figure 16 shows changes in bulk BEC on August 26, 2022. The imaging results are like those from August 19, with continued development of a dominant flow path through the backfill materials to the Hanford formation through the deepest part of the pit boundary in the western half of the imaging zone (cross-sections D-F). Figure 16 is representative of conditions that persisted through the end of September, when soil flushing stopped, with only small variations in flush water distribution occurring when switching between the west and east flush zones.

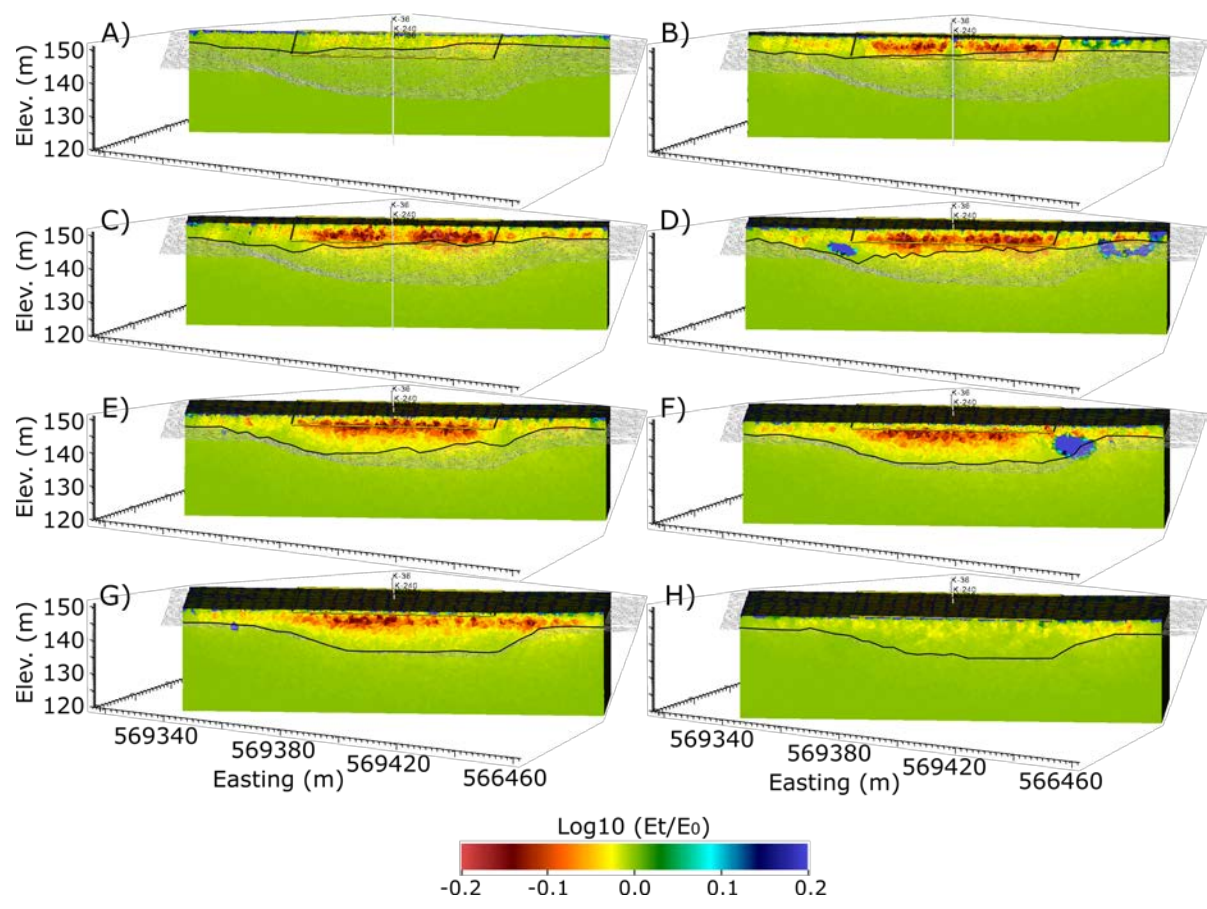


Figure 17. ERT image from November 30, 2022.

Figure 17 shows the change in bulk BEC from baseline on November 30, 2022, ~2 months after flush water application ceased. Flush water appears to have drained at least to below the imaging depth of the ERT array, (~130-m elevation), as evidenced by the lack of positive conductivity anomalies (except for the small unexplained anomalies in cross-sections D and F). The negative near-surface anomalies are likely a temperature effect, as surface soil temperatures were likely cooler in November than in June when baseline was collected.

## 7.0 2023 Imaging Summary and Interpretation

This section summarizes the ERT monitoring results for the 2023 100-KE Area soil flushing campaign and provides interpretation of the images. Figure 18 shows the timeline and dates of ERT images presented in this section with respect to flush water application rates. Each image time was chosen to highlight flush water dynamics due to changing application rates and locations, and the effects hydrogeologic heterogeneity beneath the flush zone. Flush water applications rates in 2023 began at ~190 lpm (50 gpm) and increased to 454 lpm (120 gpm) over an 8-week period from April 1 to May 22, 2023 (Figure 18). From May 22 to June 22, application rates were sustained at 454 lpm (120 gpm), which is more than twice the sustained 2022 application rate. Soil flushing was halted on June 22, 2023, although ERT monitoring continued through June 26, when the last ERT survey was collected.

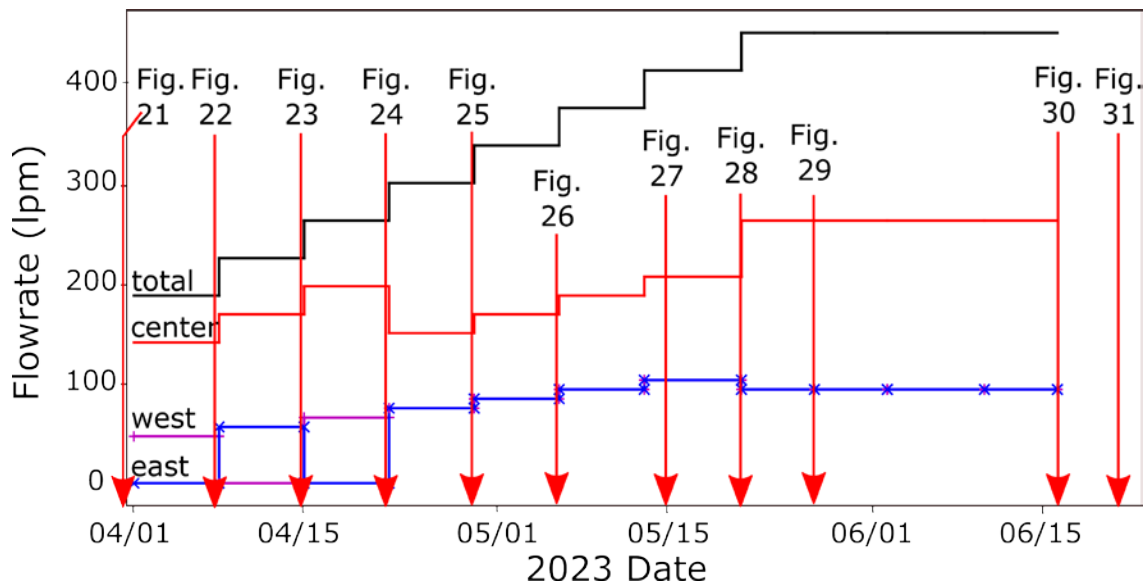


Figure 18. Times and dates of 2023 ERT images presented in section and corresponding flush water application rates.

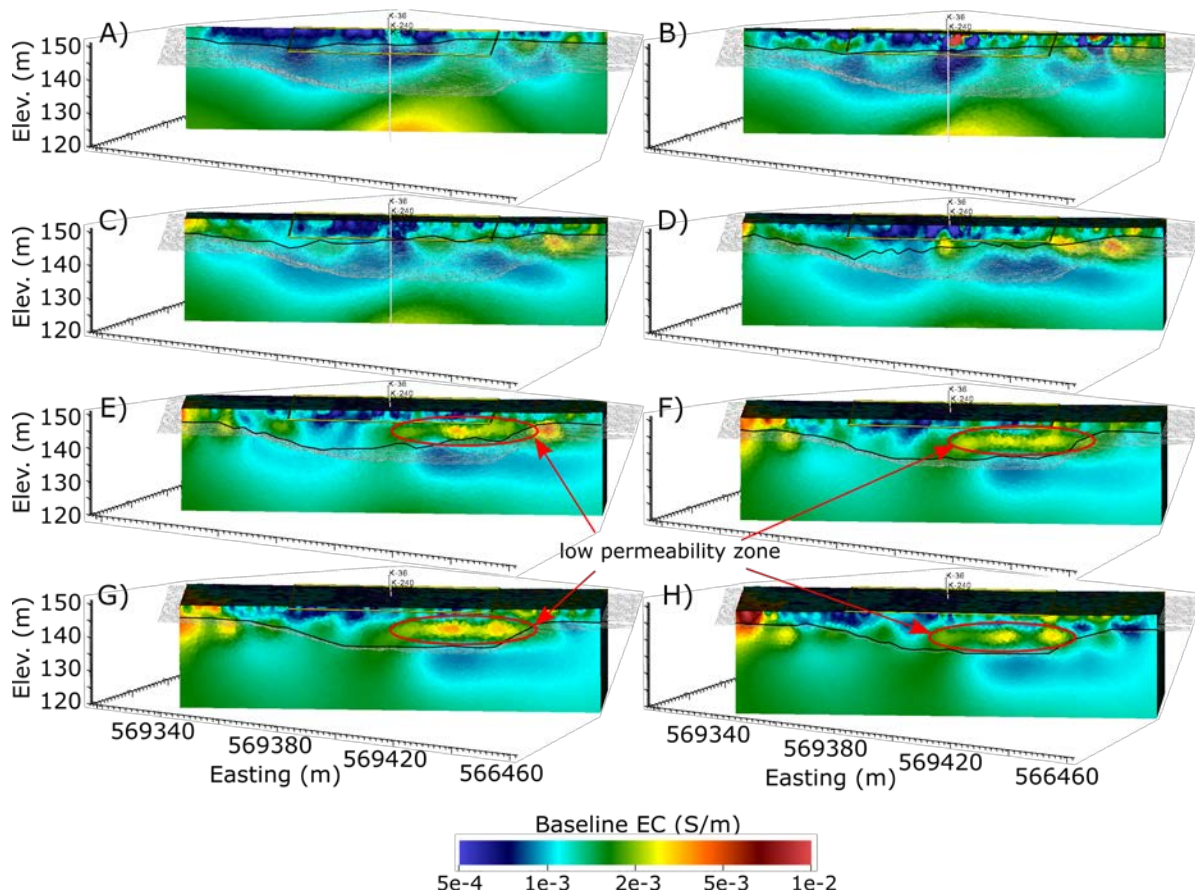


Figure 19. 2023 baseline ERT image from March 30, 2023.

Figure 19 shows the 2023 baseline ERT image from March 30, 2023, 1 day prior to the initiation of soil flushing on April 1, 2023. Results are generally like the 2022 baseline images, with minor differences that may have been caused by 2022 soil flushing. The baseline image is subtracted from every subsequent image collected during soil flushing to reveal increases in BEC associated with increases in soil saturation over time. Spatial variations in BEC within the baseline image may be caused variations in porosity, soil saturation, pore fluid conductivity, or soil texture. Absolute BEC variations cannot be uniquely attributed to any single property without supporting information. However, transient changes in bulk BEC can often be uniquely attributed to a single process such as the increase in saturation caused by soil flushing in this case. Like the 2022 baseline image (Figure 10), Figure 18 highlights an elevated region of baseline bulk BEC within the pit backfill, which appears to be a low-permeability zone that impedes vertical migration of flush water through the pit materials.

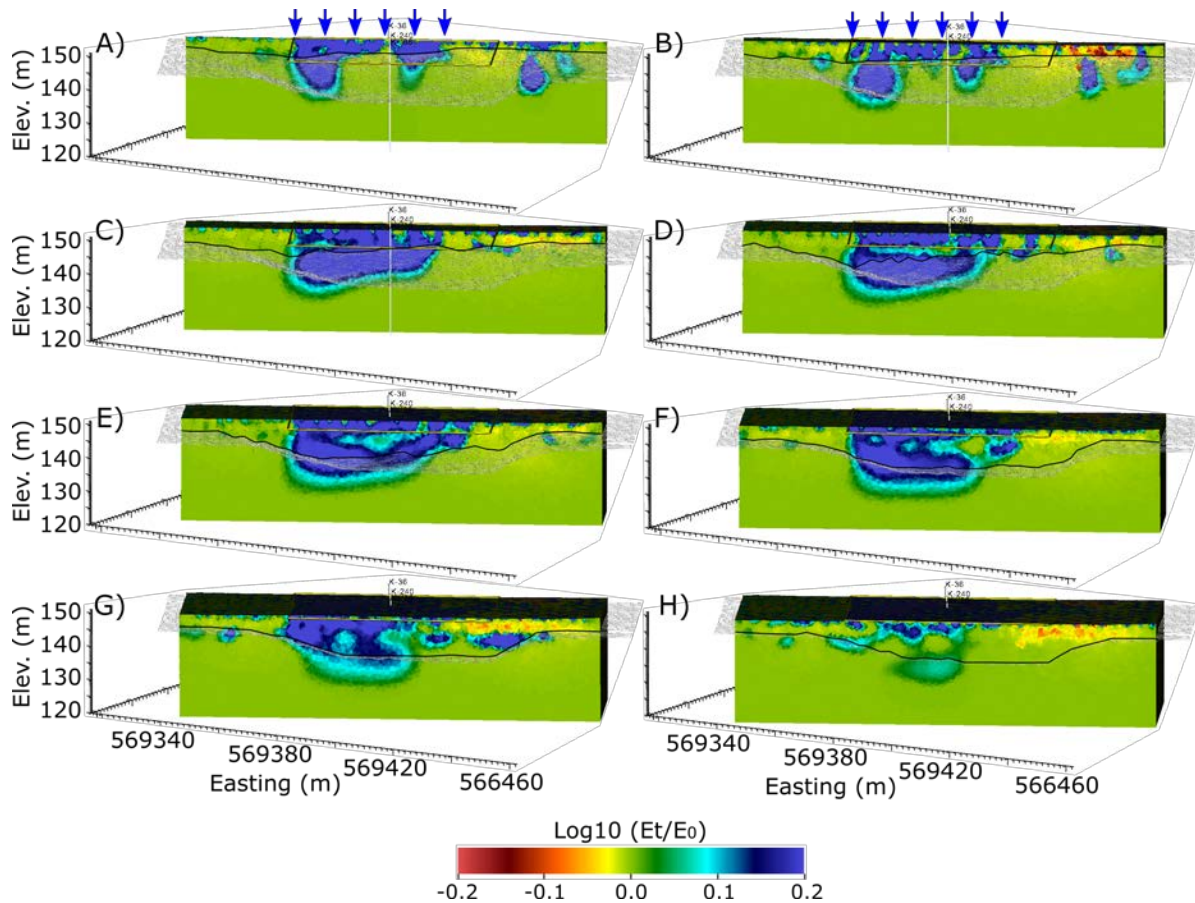


Figure 20. ERT image from April 8, 2023, after 1 week of soil flushing.

Figure 20 shows the flush water distribution on April 8, 2023, after 1 week of flush water application to the center and western flushing zones (Figure 18). Vertical migration of flush water is clearly impeded by the relatively shallow pit boundary in cross-sections A and B in comparison to cross-sections C-F, suggesting that some of the flush water applied at cross-sections A-B is likely migrating downward along the pit boundary to cross-section C. Flush water is flowing into the Hanford formation in cross-sections C and D, although it is apparent the water is redistributed along the pit boundary. For example, in cross-section C (and D to a lesser extent), the slope of the flush water front within the Hanford formation mimics the slope of the pit boundary. Likewise, the leading front of flush water in cross-sections E and F mimics the shape of the pit boundary. As observed in the 2022 imaging data, vertical migration of flush water appears to be increasingly impeded by lower permeability backfill materials moving from cross-sections G to H. Cross-sections G-H show a relatively thin horizontal layer within the backfill materials that is not penetrated by flush water, suggesting the layer is low permeability and is likely redirecting flush water within the backfill materials. The same layer is highlighted in the baseline image (Figure 19).

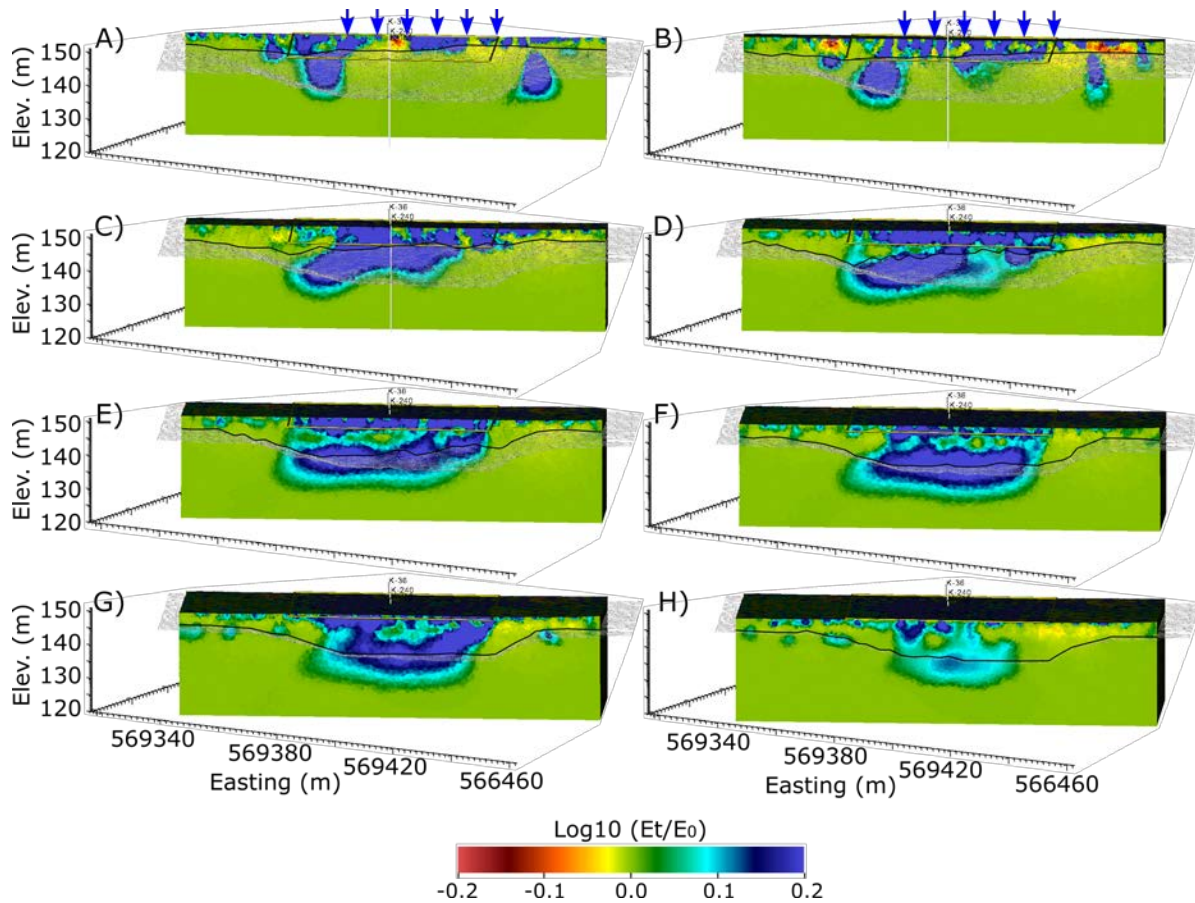


Figure 21. ERT image from April 15, 2023, after 2 weeks of soils flushing.

Figure 21 shows the change in BEC from baseline collected on April 15, 2023, 1 week after flush water application was switched from the western zone to the eastern zone, with continuous flushing in the central zone. In addition, application rates were increased in comparison to the previous week (Figure 18). Cross-sections A-D are like April 8, except more flush water is present beneath the eastern flush zone (i.e., where the flush water is being applied). Cross-sections E-F show strong evidence of flush water redistribution along the pit boundary at the bottom of the pit. Continuous vertical flow pathways appear to have developed in cross-sections G and H, although the effect of low-permeability backfill materials is evident (i.e., there is less flush water in cross-sections G and H than in cross-sections E and F). Of all images collected in 2022 and 2023, the April 15 image (Figure 21) displays the most convincing evidence of flush water redirection along the boundary between pit backfill materials and the Hanford formation. Vertical migration appears to be impeded at the pit boundary, with some water being redirected along the interface toward the bottom of the pit.

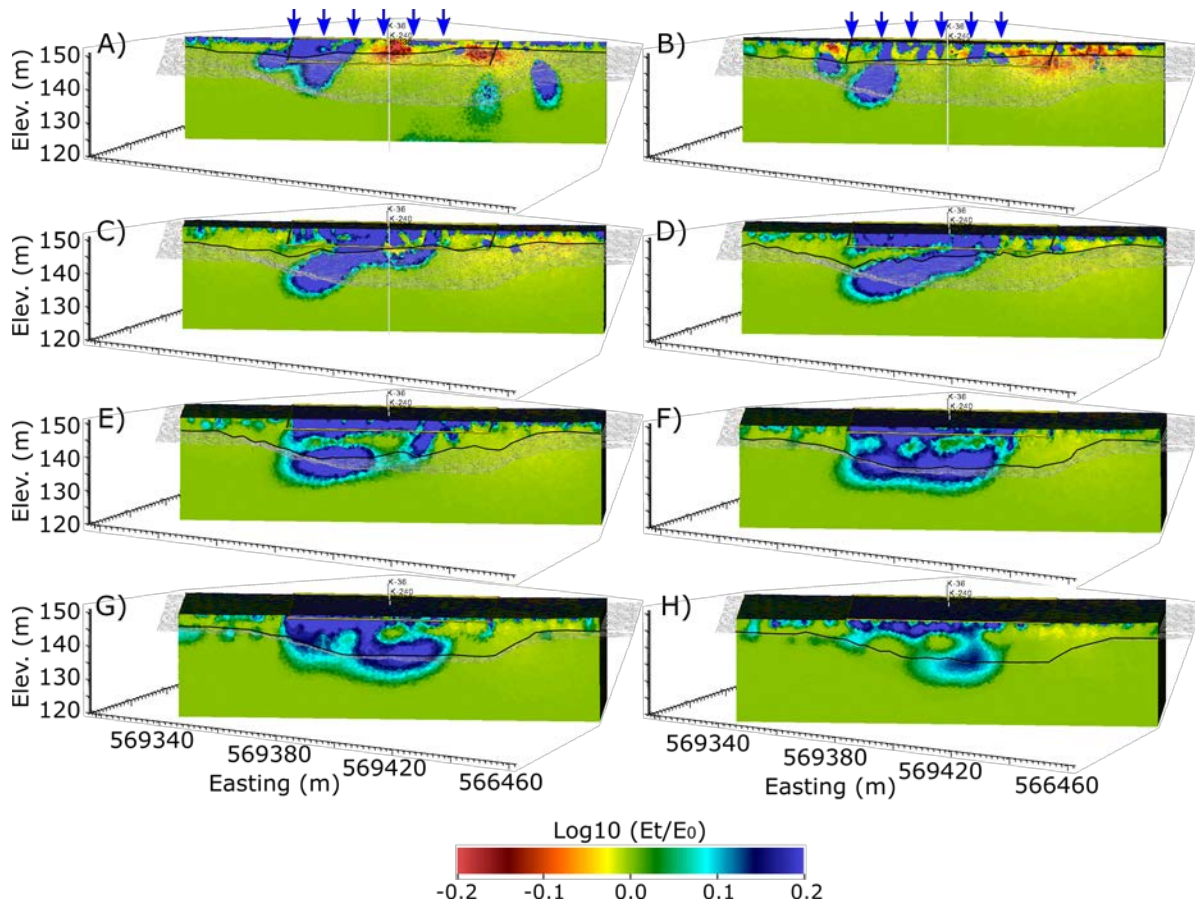


Figure 22. ERT image from April 27, 2023, after 3 weeks of soil flushing.

Figure 22 shows the change in BEC on April 22, 2023. In the preceding week, flush water was applied in the western and central flush zones, with an increased application rate in the central flush zone compared to the previous week (Figure 18). Results are like those of April 15 with two primary differences. First, there is naturally less flush water beneath the eastern flush zone in all cross-sections. Second, flush water distribution beneath cross-sections A and B appears to have decreased significantly in comparison to previous weeks. One possible explanation is the development of preferred flow pathways, as observed during the 2022 flushing campaign. For example, some portion of the flush water is clearly flowing into relatively focused regions of Hanford formation beneath the western flush zone in cross-sections A and B. In cross-section B, there appear to be localized regions of flush water above the pit boundary that do not migrate into the Hanford formation. These may be focused flow pathways transporting some flush water along the pit boundary toward cross-section C.

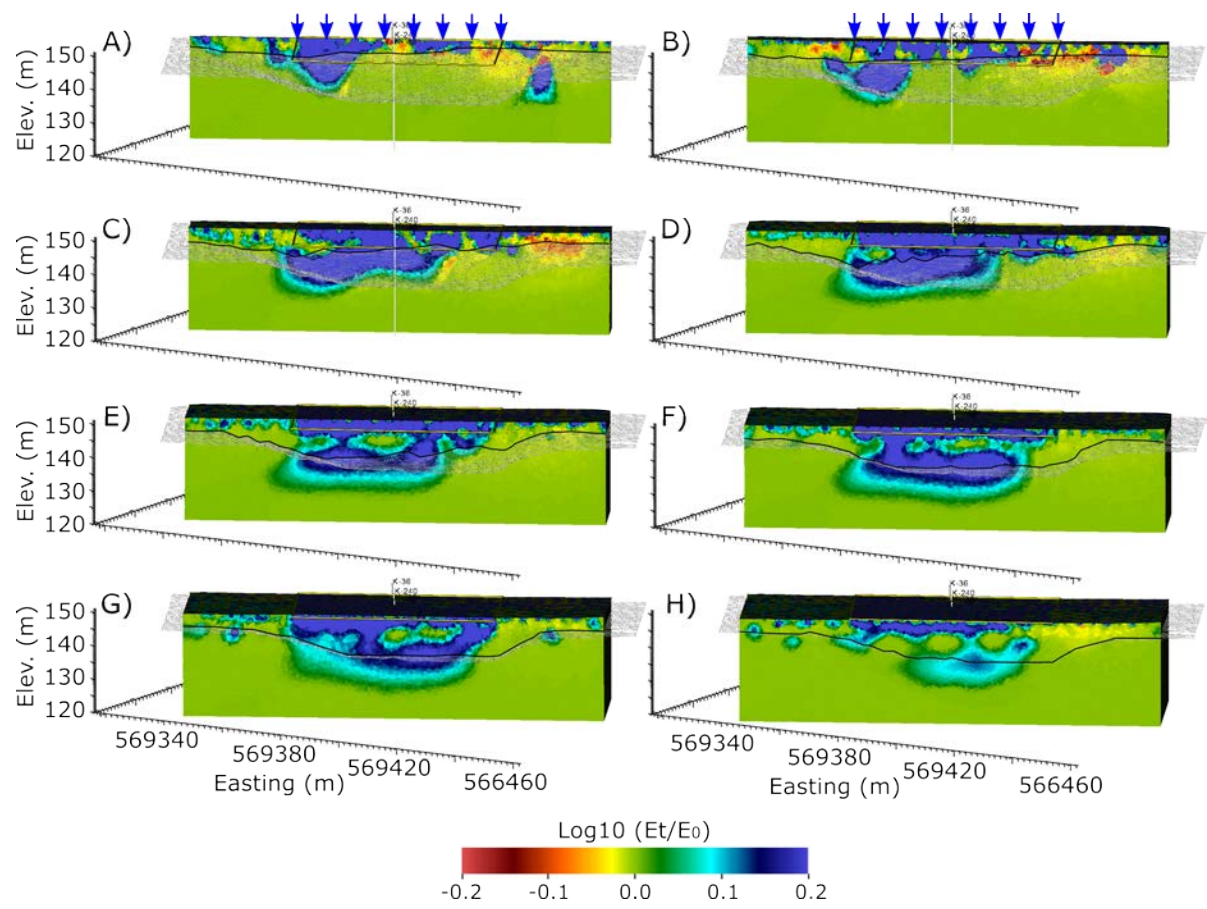


Figure 23. ERT image from April 29, 2023, after 4 weeks of soil flushing.

Figure 23 shows the change in BEC from baseline on April 29, 2023. During the preceding week, flush water was applied in all three flush zones for the first time, with an increased total application rate compared to the week of April 22 (Figure 18). Results are like the week of April 22 (Figure 22), except for the increase in flush water beneath the eastern flush zone in all cross-sections.

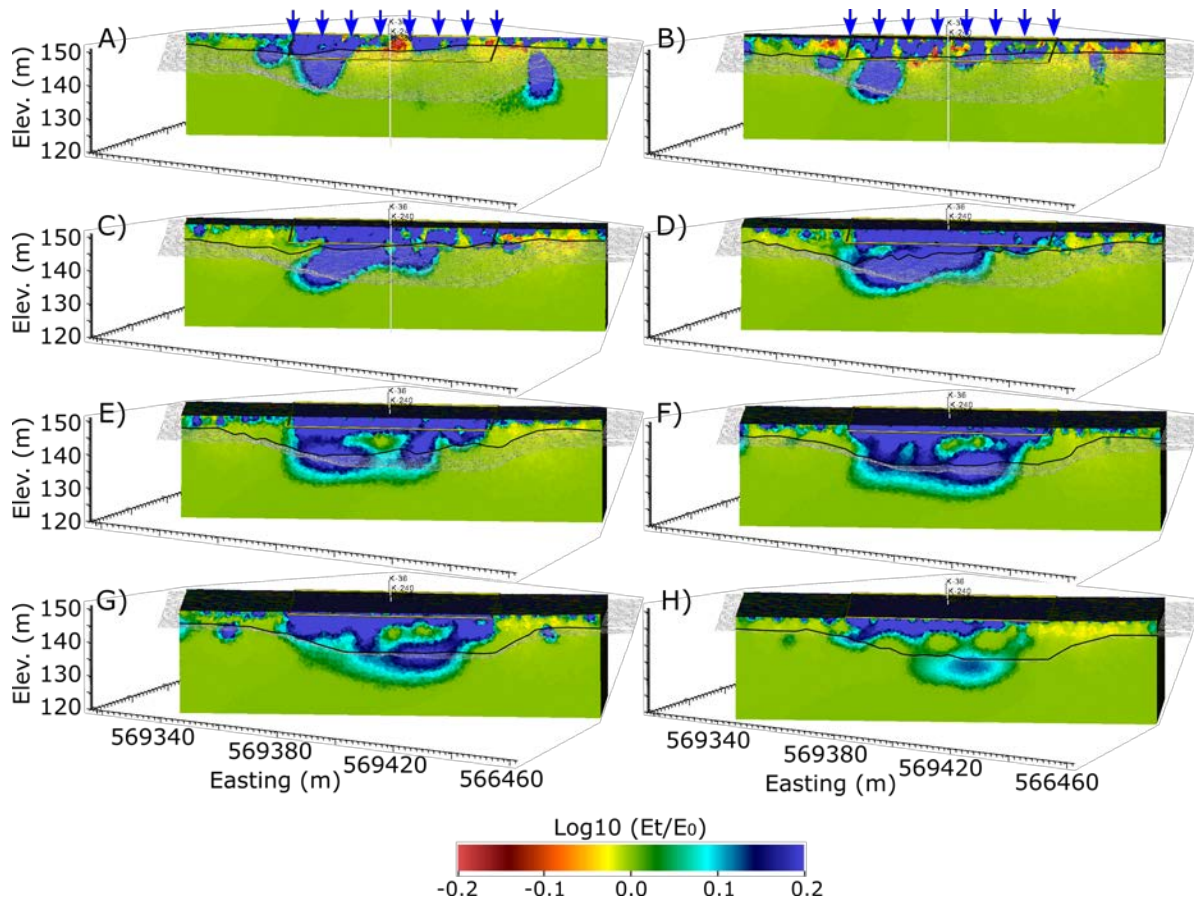


Figure 24. ERT image from May 6, 2023, after 5 weeks of soil flushing.

Figure 24 shows the change in BEC from baseline on May 6, 2023, after 5 weeks of flushing, with 2 weeks of continuous flushing in all three flushing zones. During the previous week, application rates were once again increased (Figure 18). The distribution of flush water is much like the April 29 image (Figure 23), with subtle increases in the footprint of flush water zone in all cross-sections. For example, the low-permeability zone within the backfill material (Figure 19 through Figure 23) is increasing in BEC, suggesting it is becoming increasingly saturated with flush water over time.

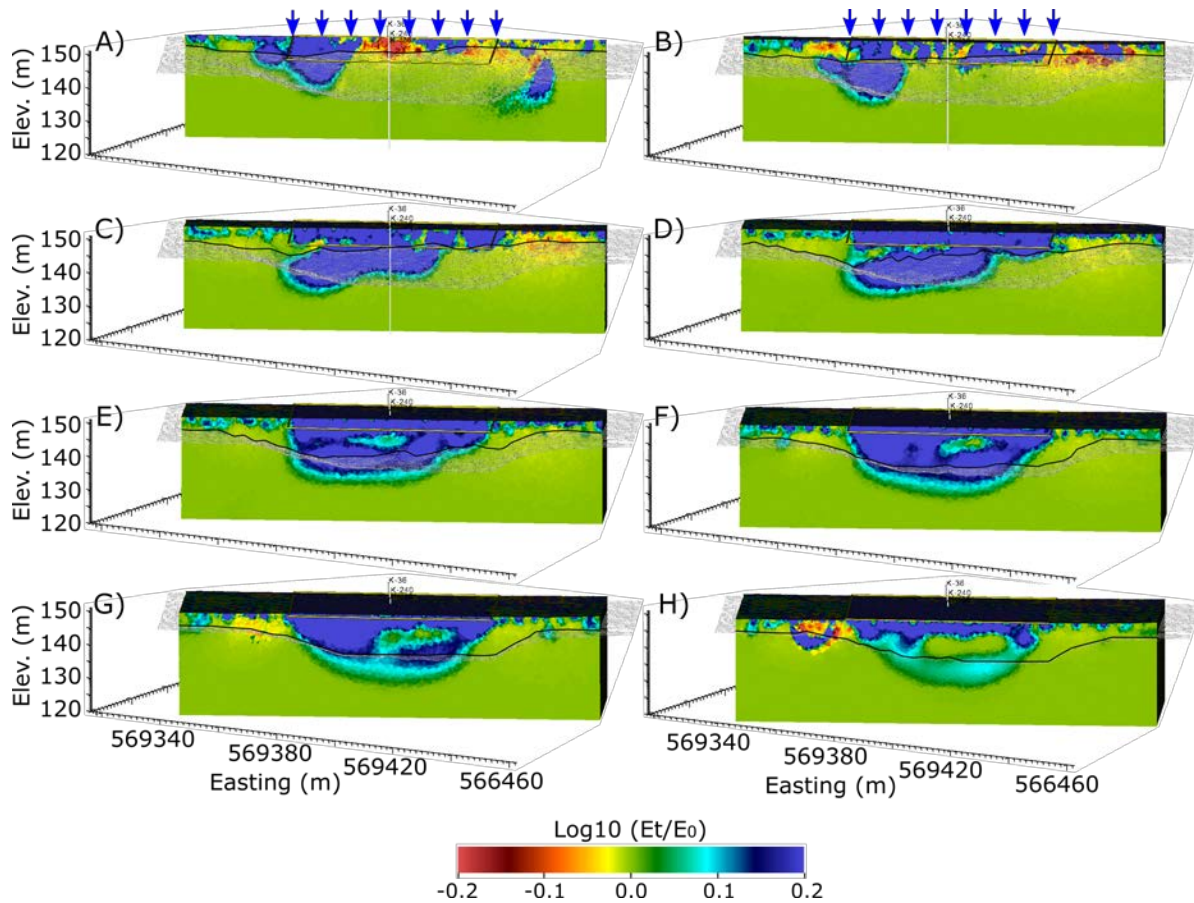


Figure 25. ERT image collected on May 15, 2023, after 6 weeks of soil flushing.

Figure 25 shows the change in BEC from baseline on May 15, 2023, after 6 weeks of flushing, with 3 weeks of continuous flushing in all three flushing zones. During the previous week, application rates were once again increased (Figure 18). Effects of increased application rates are becoming more evident as the distribution of flush water has expanded in each cross-section. Cross-sections A and B continue to show evidence of preferential flow paths and vertical flow impeded by the pit boundary. Backfill materials in cross-sections G and H show larger zones of increased BEC in comparison to the previous week, suggesting they are slowly being infiltrated with flush water in comparison to the faster backfill flow rates exhibited in cross-sections A-F. The low-permeability zone within the backfill material (Figure 19 through Figure 23) also continues to increase in BEC, suggesting it is becoming increasingly saturated with flush water over time.

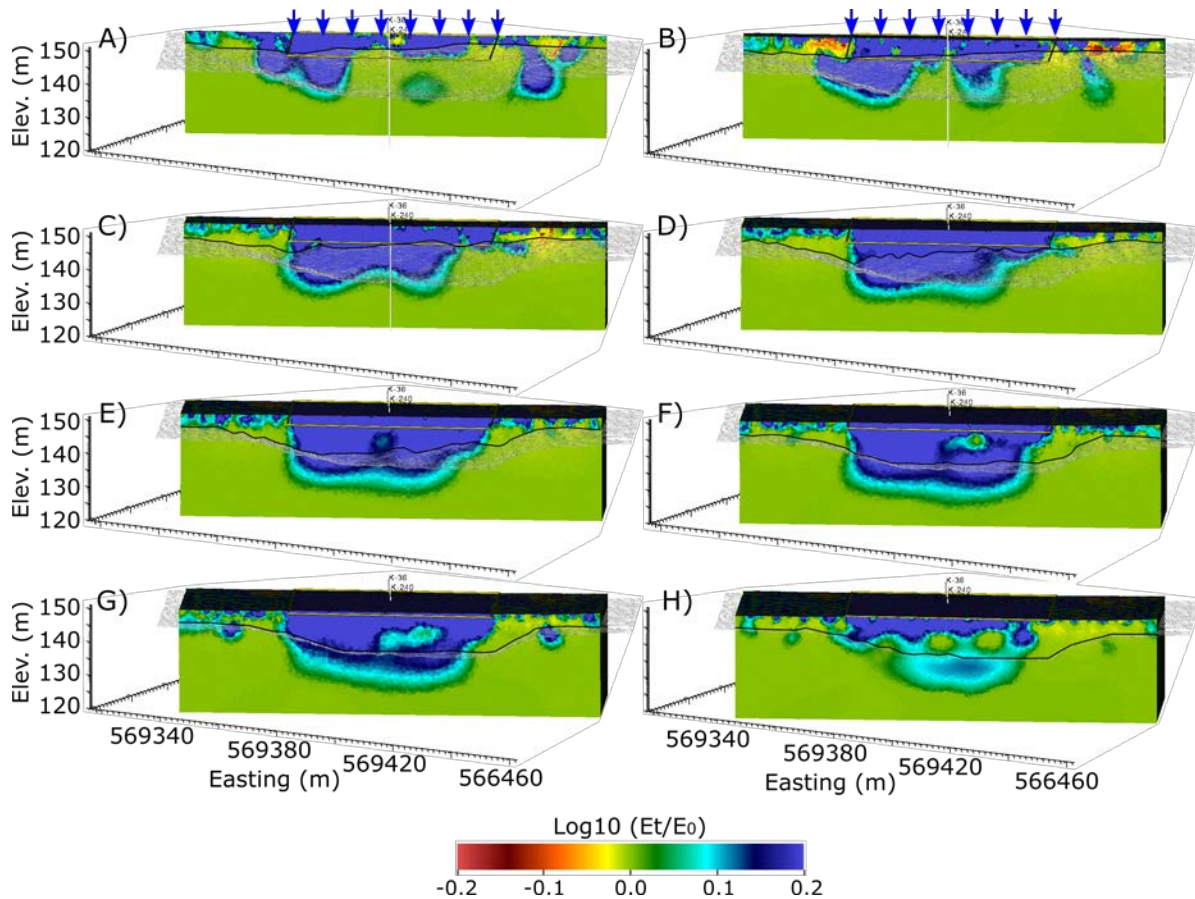


Figure 26. ERT image from May 22, 2023, after 7 weeks of soil flushing.

Figure 26 shows the change in BEC from baseline on May 22, 2023, after 7 weeks of flushing, with 4 weeks of continuous flushing in all three flushing zones. During the previous week, application rates were again increased in comparison to May 15 (Figure 18). The impact of weekly increases in application rate is strongly evident on May 22. Regions of increased BEC have expanded in every cross-section. It is also apparent that greater volumes of flush water are flowing through the pit boundary to the Hanford formation in cross-sections A and B. Note that vertical migration of flush water appears to be impeded near the extraction well in cross-sections A and B. This may be an artifact of reduced imaging sensitivity due to the metallic wellbore casing and consequent equalization of subsurface electrical potentials at the casing boundary. Flush water may be migrating deeper into the formation near the wellbore than is suggested by Figure 26.

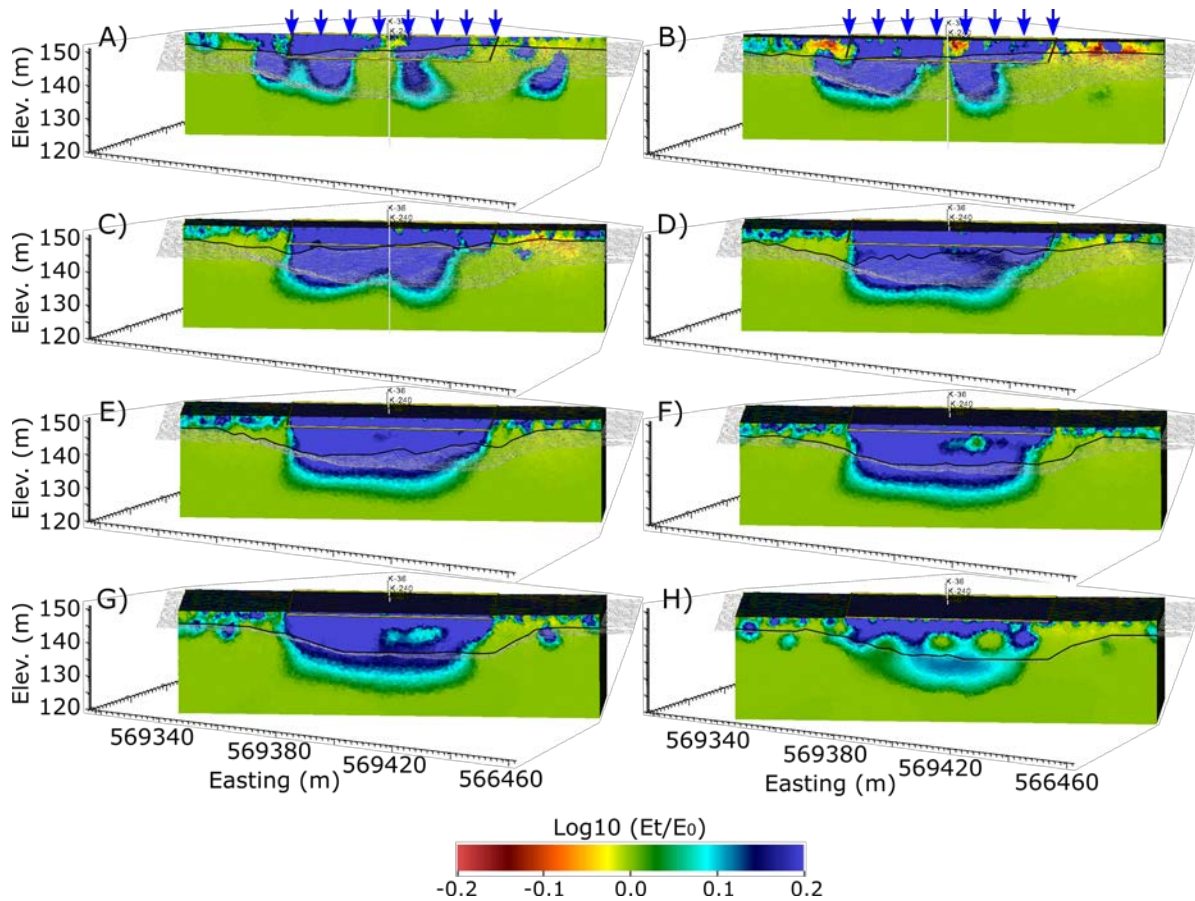


Figure 27. ERT image from May 29, 2023, after 8 weeks of soil flushing.

Figure 27 shows the change in BEC from baseline on May 29, 2023, after 8 weeks of flushing, with 5 weeks of continuous flushing in all three flushing zones. During the previous week, application rates were raised to their highest level of 454 lpm (120 gpm), and this rate was sustained through the end of soil flushing on June 22 (Figure 18). The previously noted trends of increases in BEC in each cross-section continue, suggesting the increased application rates significantly improved the distribution of flush water in all cross-sections in comparison to 2022.

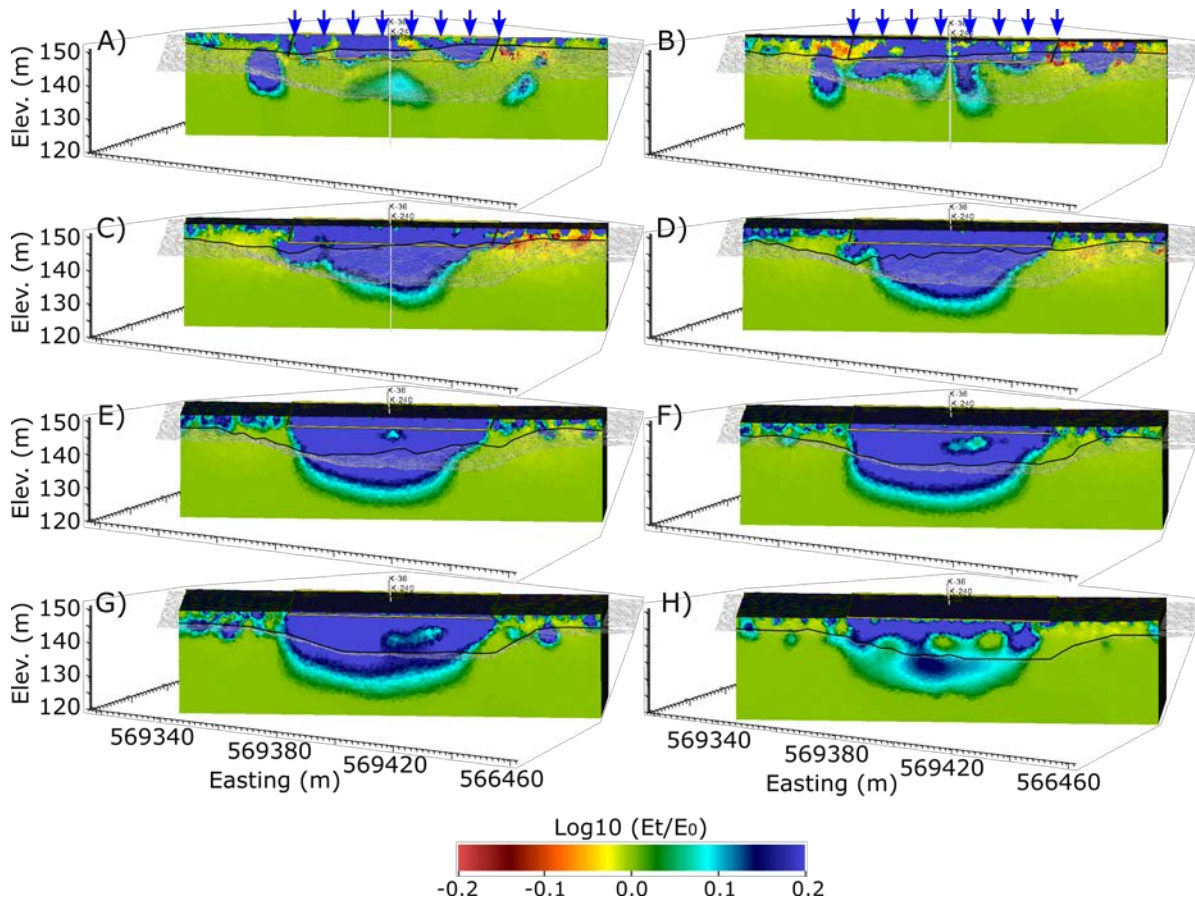


Figure 28. ERT image from June 20, 2023, after 11 weeks of soil flushing.

Figure 28 shows the change in BEC from baseline on June 20, 2023, after 8 weeks of continuous flushing in all three flushing zones, with the final 4 weeks of flushing at the highest application rate used in the 2022 and 2023 flushing campaigns (454 lpm, 120 gpm). In comparison to 2022, higher application rates have significantly improved flushed water distribution, and presumably the efficacy of soil flushing overall, particularly along the inner cross-sections (C-G). Vertical migration of flux water beneath in cross-sections A and B is also improved compared to lower flush rates but is still clearly impeded at the pit boundary. Vertical migration within cross-section H is also significantly improved compared to lower application rates but is slowed by the apparent lower permeability materials within the backfill zone.

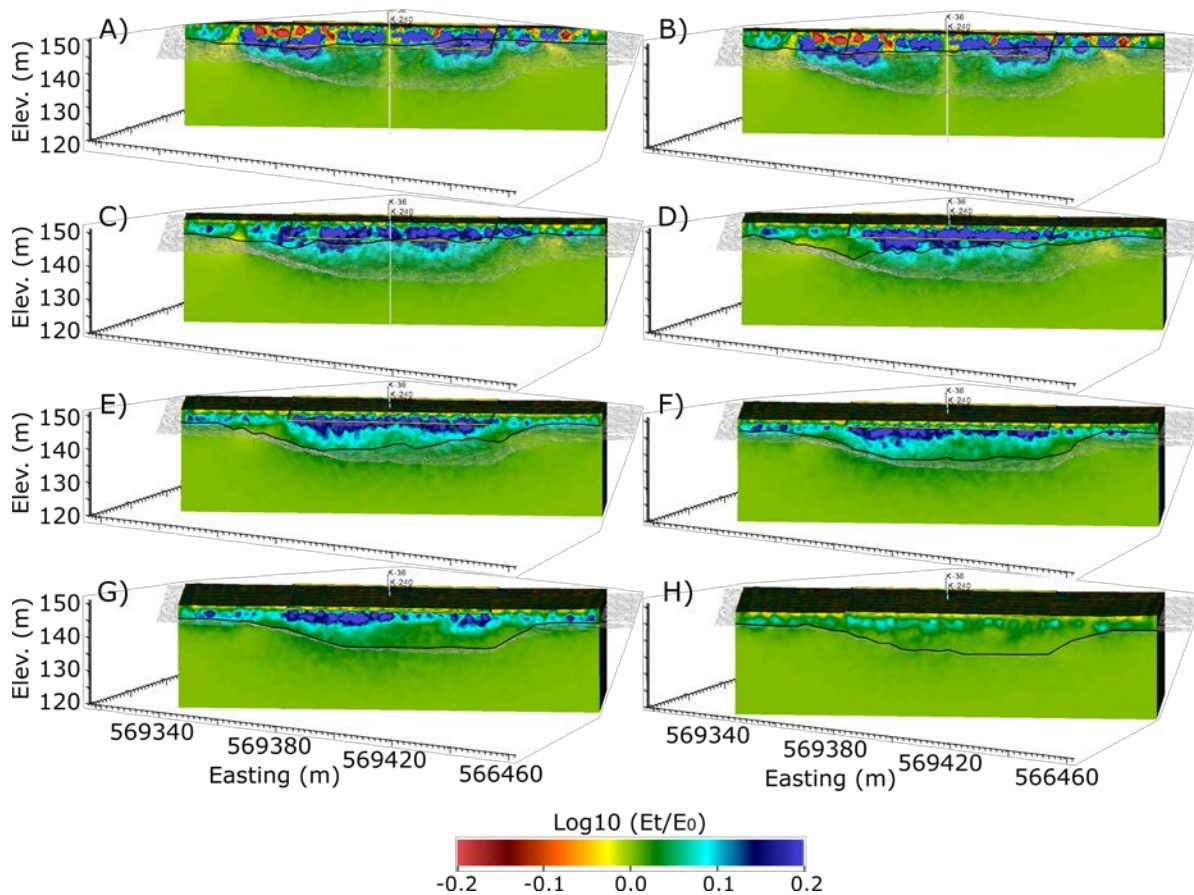


Figure 29. ERT image from June 26, 2023, 4 days after the end of soil flushing.

Figure 29 shows the change in BEC from baseline on June 26, 2023, 4 days after flush water application ended. In comparison to Figure 28, it is apparent that most of the flush water has drained to beneath the depth of resolution (~130 m). Shallow increases in BEC in comparison to the baseline present in each cross-section may be caused by increased ambient temperatures and/or the increased temperature of flush water over time. Both of these could have resulted in higher soil temperatures in the shallow subsurface on June 26 in comparison to baseline conditions on April 1, and therefore an increase in shallow BEC relative to baseline.

## 8.0 Discussion and Conclusion

Interpretations of the ERT images provided in Sections 6.0 and 7.0 assume flush water is evenly distributed at the surface within the flush zone boundary. Uneven distribution of flush water, depending on severity, could cause some of the uneven distributions of flush water observed in the ERT images. Flush water temperature is also assumed to be relatively constant over time, although flush water temperature may have risen with ambient air temperatures over the spring and summer months (i.e., during transport within overland delivery piping). The effects of increasing flush water temperatures would likely be manifest as increases in near-surface BEC, as flush water temperatures and soil temperatures would likely equilibrate in the shallow subsurface. Temperature effects are not expected to influence imaging results in the targeted flush water delivery zones within the Hanford formation.

Under these assumptions, five primary conclusions are derived from the ERT monitoring of the 2022 and 2023 soil flushing campaigns:

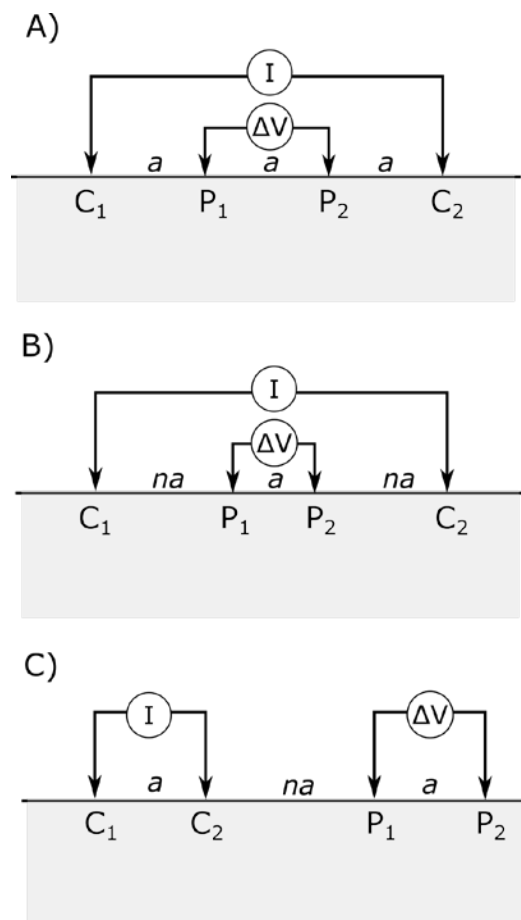
1. Pit backfill materials appear to nominally have larger permeability than native soils. Consequently, the boundary between pit backfill and native soil had a significant impact on flush water migration, causing some flush water to migrate along the pit boundary to the bottom of the pit.
2. Non-uniform flows, likely caused by variations in hydrogeologic properties, developed in the pit backfill materials, resulting in uneven flush water distribution on the southern margin of the soil flushing zone.
3. Redistribution of water at the interface between backfill materials and the underlying Hanford formation sediments likely facilitated enhanced flushing within native soils beneath the deeper parts of the pit boundary, which presumably overlies soils with elevated Cr(VI) contamination. These areas appear to have been infiltrated by higher volumes of flush water than the northern and southern margins of the flush zone.
4. In comparison to 2022, high flush water application rates significantly improved flush water distribution throughout the target flushing zone.
5. Imaging resolution was limited to a depth of ~20 m below the land surface, due primarily to limitations on the lateral extent of the surface ERT array. The ~10-m region of the vadose zone between approximately 130-m elevation and the water table at ~120-m elevation was unresolved.

## 9.0 References

- Glass, R. J., S. Cann, J. King, N. Baily, J. Y. Parlange, and T. S. Steenhuis. 1990. "Wetting Front Instability in Unsaturated Porous-Media - a 3-Dimensional Study in Initially Dry Sand." *Transport in Porous Media* 5 (3):247-268. doi:10.1007/Bf00140015.
- Jarvis, N., J. Koestel, and M. Larsbo. 2016. "Understanding Preferential Flow in the Vadose Zone: Recent Advances and Future Prospects." *Vadose Zone Journal* 15 (12). doi:10.2136/vzj2016.09.0075.
- Johnson, T. C., and D. Wellman. 2015. "Accurate modelling and inversion of electrical resistivity data in the presence of metallic infrastructure with known location and dimension." *Geophysical Journal International* 202 (2):1096-1108. doi:10.1093/gji/ggv206.
- Johnson, T. C., Y. Zhu, and J. Robinson. 2020. *Feasibility and performance assessment for ERT monitoring of proposed 100-KE Soil Flushing*. PNNL-30552, Pacific Northwest National Laboratory, Richland, WA.
- Szecsody, J., H. Emerson, A. Lawter, C. Resch, M. Rockhold, R. Mackley, N. Quofoku. 2023. "Vadose zone flushing for chromium remediation: a laboratory investigation to support field-scale application." *Groundwater Monitoring & Remediation (accepted)*. doi:10.1111/gwmr.12570
- Szecsody, J.E., N. Qafoku, A.R. Lawter, R.D. Mackley, H.P. Emerson, and C.T. Resch. 2022. *Laboratory Evaluation to Increase Effectiveness of Field-Scale Soil Flushing in the Hanford 100 Areas*. PNNL-31980, rev 1. Pacific Northwest National Laboratory, Richland, WA.

## Appendix A – ERT Methods

Data collection was conducted using a Pacific Northwest National Laboratory-approved operating procedure and safety protocol. A single electrical resistivity tomography (ERT) measurement involves injecting current ( $I$ ) between one electrode pair and measuring the resultant electrical potential (i.e., the voltage,  $\Delta V$ ) across a second (or more) electrode pair(s). Raw ERT data are provided to the inversion algorithm as the observed voltages normalized by the injected currents ( $\Delta V / I$ ) and have units of resistance (ohms). Many such measurements are strategically chosen to optimize imaging resolution.



ERT measurements collected during the 100-KE soil flushing campaigns included a comprehensive series of Wenner-Alpha and dipole-dipole type four-electrode configurations (Figure A.1). Small-offset dipoles (electrodes pairs in close proximity to each other, where  $a$  and  $na$  are small) provide high resolution in the vicinity of the electrodes and constrain near-surface structures in the ERT inversion. Large offset dipoles (large  $n$  and  $na$ ) probe deeper into the subsurface. Comprehensive combinations of small, intermediate, and large offset dipoles used in the survey were implemented to optimize resolution for both shallow and deep structures to the extent possible. The survey was also optimized to leverage the eight channels available in the data collection system; eight different potential electrode pairs were recorded for each current electrode pair. In total, 4730 measurements were collected per ERT survey.

Data quality was assessed by reviewing contact resistances, current injections, and stacking deviations for each measurement. Using conservative boundaries for these values, outlier measurements were removed.

Data quality was assessed by collecting repeat surveys on the days prior to the onset of soil flushing. In theory, these measurements should be equal, and differences can be attributed to data noise. Measurements whose standard deviation exceeded 10% of the mean value were excluded from collection. Only 22 such measurements were identified, meaning 4708 measurements were collected per survey during ERT monitoring.

Figure A.1. Electrode measurement configurations used in the ERT survey including A) Wenner-Alpha, B) Schlumberger, and C) dipole-dipole. C1 and C2 are current source and sink, respectively. P1 and P2 are the potential source and sink, respectively.

## A.1 ERT Imaging Resolution

ERT images are limited in resolution. Consequently, small-scale features may not be resolved, and larger resolvable features will be manifest as smoothed or blurred versions of the actual subsurface bulk electrical conductivity (BEC). Imaging resolution is governed by many factors, including electrode spacing, proximity to electrodes, background electrical noise, and measurement sequence. BEC distribution also impacts imaging resolution as this controls how and where electrical current flows in the subsurface. For example, if a deeper, low-conductivity layer is overlain by a shallower, high-conductivity layer, the bottom layer may have limited resolution due to a lack of current penetration in the lower layer. Inclusion of known geologic contacts (e.g., Cold Creek Unit and Hanford formation) in the ERT modeling can improve imaging resolution; however, there must be strong evidence of the location of these boundaries as misplacement can lead to misinterpretation. For a surface ERT array, resolution decreases with depth. Resolution cannot be quantified prior to collecting field data.

ERT survey design is the process of choosing electrode locations and which ERT measurements should be collected to optimally resolve targeted subsurface locations. This is based on assumed conditions and trial-and-error synthetic imaging experiments. One such representative experiment is shown in Figure A.2. A target BEC anomaly was placed in the subsurface and ERT imaging was simulated using a comprehensive set of ERT measurements. The targets and ERT images demonstrate the effects of limited resolution. Namely, the near-surface target is better resolved than the deeper target because it is closer to the electrodes. Both targets are clearly detected and imaged, but the images are blurred and have a larger footprint than the actual targets. Limited resolution effects such as these are important to consider when interpreting 100-KE Area ERT images. In particular, the footprints of BEC anomalies are likely to be larger in the ERT images than they are in reality, and the outer extents of anomalies will typically bound the true extents, assuming the anomalies are within the zone of investigation.

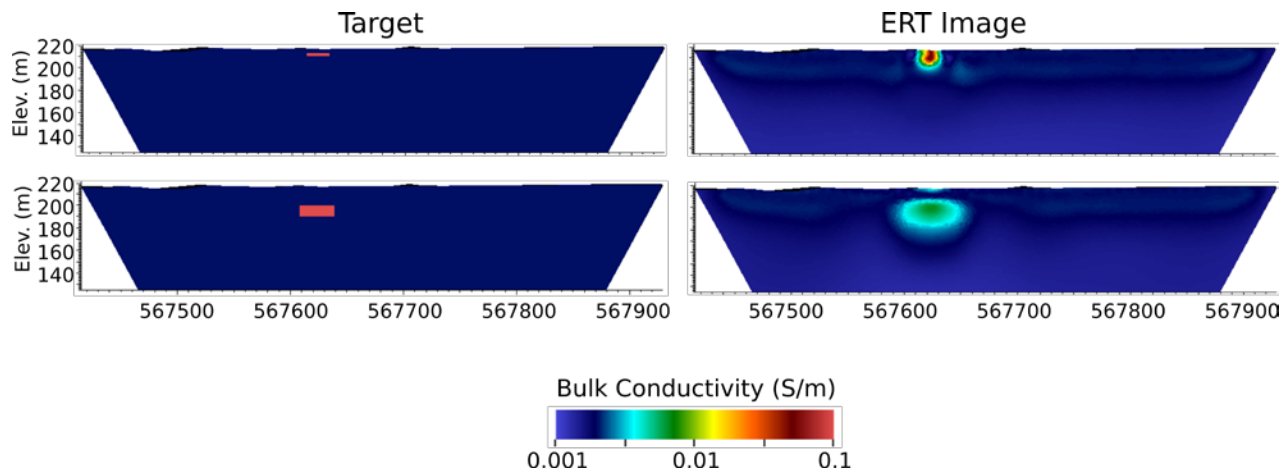


Figure A.2. Synthetic imaging example demonstrating the effects of limited resolution.

# **Pacific Northwest National Laboratory**

902 Battelle Boulevard  
P.O. Box 999  
Richland, WA 99354

1-888-375-PNNL (7665)

***[www.pnnl.gov](http://www.pnnl.gov)***